

NASA CR-132574
February 1975

FINAL REPORT

VIDEO GUIDANCE, LANDING, AND IMAGING SYSTEM (VGLIS)
FOR SPACE MISSIONS

By Roger T. Schappell, Robert L. Knickerbocker,
John C. Tietz, Christopher Grant, and John C. Flemming

(NASA-CR-132574) VIDEO GUIDANCE, LANDING,
AND IMAGING SYSTEM (VGLIS) FOR SPACE
MISSIONS Final Report (Martin Marietta
Corp.) 69 p HC \$4.25 CSDL 14B

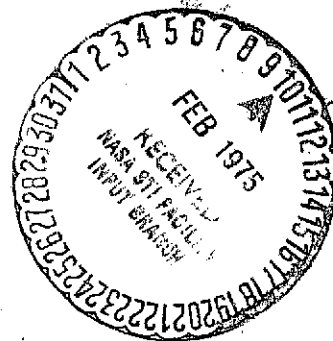
N75-16444

63/91 Unclas
07756

Prepared under Contract No. NAS1-13558 by
MARTIN MARIETTA CORPORATION
Denver, Colorado 80201

for

NATIONAL AERONAUTICS AND SPACE ADMINISTRATION
Langley Research Center, Hampton, Virginia 23365



FINAL REPORT

VIDEO GUIDANCE, LANDING, AND IMAGING SYSTEM (VGLIS)
FOR SPACE MISSIONS

By Roger T. Schappell, Robert L. Knickerbocker,
John C. Tietz, Christopher Grant, and John C. Flemming

Prepared under Contract No. NAS1-13558 by
MARTIN MARIETTA CORPORATION
Denver, Colorado 80201

for

NATIONAL AERONAUTICS AND SPACE ADMINISTRATION
Langley Research Center, Hampton, Virginia 23365

FOREWORD

This report presents the results of a five-month video guidance, landing and imaging system feasibility study. It summarizes both the laboratory and digital simulation results arrived at in the process of establishing and performing the feasibility demonstration.

CONTENTS

	Page
SUMMARY	1
INTRODUCTION	4
SYSTEM OPERATION	6
Flight System	6
Laboratory System	8
SURFACE MODEL	21
EXPERIMENTAL RESULTS	26
Calibration	26
Algorithm Evaluation Experiments	32
Monte Carlo Experiment	37
MISSION CONSIDERATIONS	40
Lander Constraints and Propulsion System	40
Impact of Additional Fuel on Propulsion System	43
Maneuver Capability	43
HARDWARE AND INTERFACE REQUIREMENTS	59
RECOMMENDATIONS	59
Mission Applications Study	61
Scientific Site Selection	61
Scientific Imaging	62
Terminal Rendezvous Guidance with Solar Bodies	63
Landmark Navigation	64
Target Acquisition and Tracking	64
Earth Resources Satellite Application	65

Figures

1	Selected Landing Sites	3
2	Reference Mission - Viking	7
3	System Operation	7
4	6-D Simulator	9
5	Control Console	9
6	PDP-9 Digital Computer	11
7	VGLIS Simulator Functional Block Diagram	12
8	Image Dissector	13
9	Digital Sweep Circuit	14
10	Video Signal Processor	18
11	Scan Layout	22

12	Surface Simulation Models	22
13	Desert Land Forms of Peru	23
14	Spatial Frequency in Object Space	28
15	MTF Measurement Scheme	30
16	Camera Modulation Transfer Functions, Minimum Laboratory Altitude	30
17	Camera Modulation Transfer Functions	31
18	Variation of Camera MTF between Subframes	31
19	Monitor Observations for a Typical Experiment	36
20	Viking Velocity - Altitude Descent Contour	42
21	Viking Maximum Maneuver Capability	45
22	Terminal Descent Guidance and Control System	46
23	Maximum Maneuver Capability - Footprints	48
24	POST Optimization Algorithm	50
25	Crossrange Maneuver Capability	52
26	Field of View Positioning Logic	55
27	Three Dimension Surface Model	56
28	MOD6MV Digital Simulation	57
29	Scan Positioning Logic	58
30	Guidance and Control System Interface	60

Tables

I	VGLIS Success Probability	39
II	POST Iteration History	53
III	Maximum Maneuver Distances	53

VIDEO GUIDANCE, LANDING, AND IMAGING SYSTEM
FOR SPACE MISSIONS

By Roger T. Schappell, Robert L. Knickerbocker,
John C. Tietz, Christopher Grant, and John C. Flemming

SUMMARY

This report documents the results of Contract NAS1-13558, Video Guidance, Landing, and Imaging System (VGLIS) for Space Missions.

The feasibility of an autonomous video guidance system that is capable of observing a planetary surface during terminal descent and selecting the most acceptable landing site was demonstrated in the laboratory. The system was breadboarded and "flown" on a physical simulator consisting of a control panel and monitor, a dynamic simulator, and a PDP-9 computer. The breadboard VGLIS consisted of an image dissector camera and the appropriate processing logic. Feasibility was established in the following manner.

Fifty experiments were performed in which a simulated Viking lander was guided by a breadboard autonomous optical guidance system to landings on a three-dimensional Martian surface Model that was relatively rough compared to nominal Viking '75 sites. In each case the descent began at a simulated altitude between 500 and 900 meters, and both the altitude and the starting position on the model were selected at random by a computer random number generator. All 50 experiments were run under computer control without human intervention, and the coordinates of the selected sites were recorded on tape but not printed. A second computer program was then used to establish whether the sites selected were good or bad. The computer read the tape and positioned the system television camera at each of the 50 selected landing sites. It also positioned the camera at a large number of sites selected entirely at random.

Two experimenters, who did not observe the experiments and had not seen what sites were selected by the system, observed the sites on the model and rated each site with their estimates of success probability. To minimize experimenter bias, selected sites and random sites were presented to them in random sequence so they did not know which they were rating. Based on each experimenter's ratings, the computer recorded "successful landings" and "crashes" for both randomly selected sites and system-selected sites. Data from this program could then be used to establish the improvement in success probability obtained by using the guidance system compared with unguided landings.

To the extent practical the experiments simulated landings by a Viking lander under typical conditions in a 416,000 square meter area with several safe landing sites and several hazardous sites. The selected landing sites for 50 experiments are illustrated on the plan view of the surface model in figure 1 by the small circles.

In the experiments the computer was used to pick initial conditions to (1) interpret guidance system output signals, (2) solve equations needed to simulate lander motion and navigation computer operation, (3) control the camera and servos to simulate flight, and (4) record experimental results. To increase system flexibility, the computer was also used to perform the functions of a small portion of the guidance hardware. This allowed several algorithms to be tested for rating the suitability of a site.

During performance of the laboratory experiments it was demonstrated that a video guidance system will repeatedly select the most acceptable landing site in a given area. The experimental statistics for 100 simulated flights performed by two experiments are as follows:

Without video guidance, only 19% of the landings were successful according to the first experimenter's ratings, and 15% were successful according to the second experimenter's ratings. Using the optical guidance system, 88% were successful according to the first experimenter's ratings, and 84% were successful according to the second experimenter's ratings. Although the system did not always choose the best possible site, it successfully avoided sites the experimenters rated as having a success probability of less than 75%. In contrast, the unguided landings were frequently in locations where success probability was essentially zero. *These experimental results indicate that a relatively simple system of this type could greatly increase the probability of mission success for unmanned planetary landers where earth control is not practical.*

Based on the results of this study, Martin Marietta recommends that:

- 1) Further algorithm evaluation experiments be performed to acquire a better understanding of the effects of varying scene conditions such as sun angle, albedo, field-of-view, and to extend the VGLIS capability to entry guidance and scientific site selection;
- 2) A mission applications study be performed to optimize the VGLIS performance for advanced planetary programs;
- 3) The acquisition and tracking aspects of the system be investigated for terminal rendezvous guidance with solar bodies;

- 4) The contrast sensing capability of the VGLIS be considered in the role of target acquisition and selection for earth resources imaging satellites.

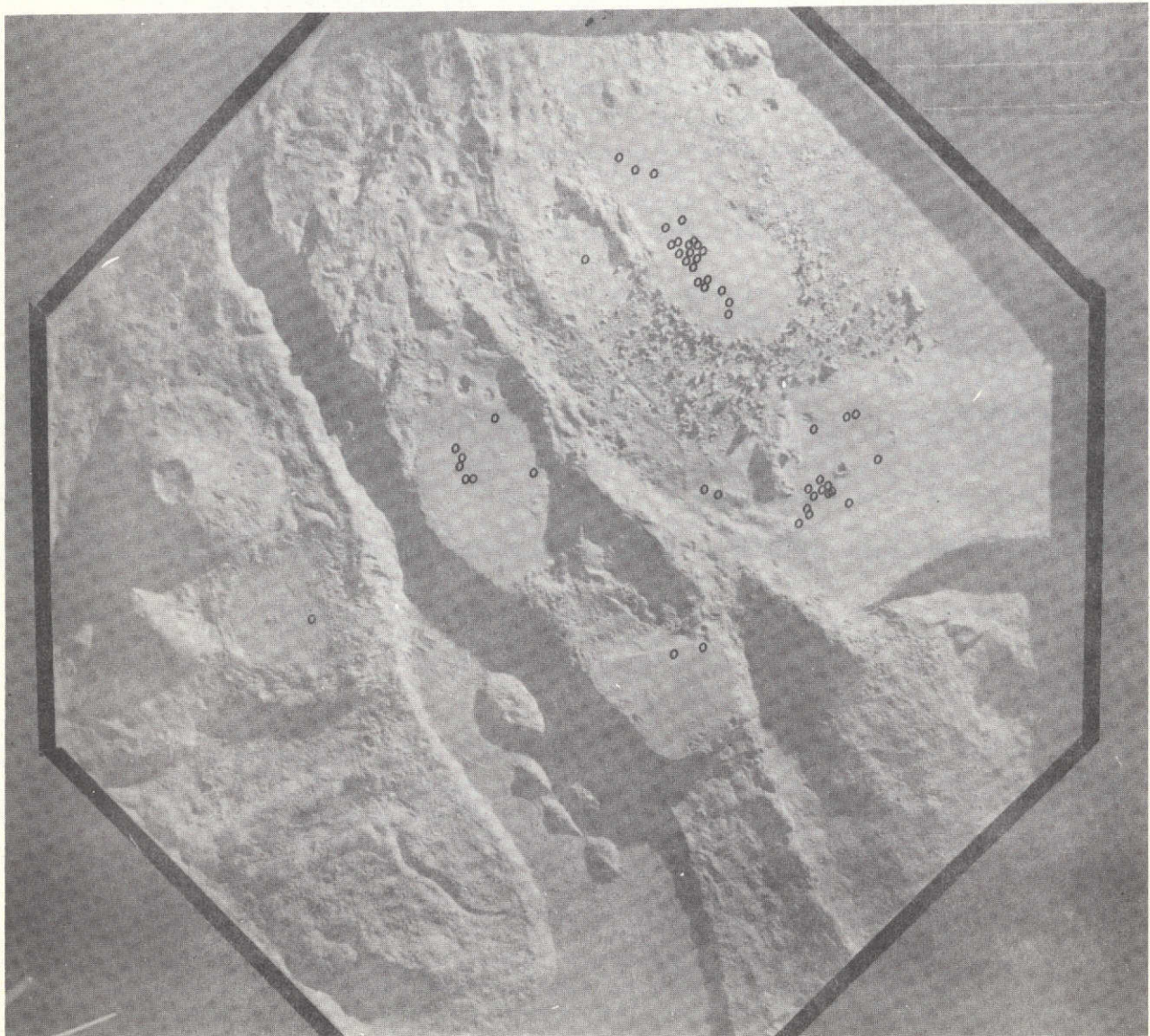


Figure 1.- Selected Landing Sites

INTRODUCTION

Traditionally, the lack of knowledge regarding the details of planetary surfaces has dictated that proposed landings of unmanned spacecraft be made in relatively benign areas. The benefits of real-time selection of a smooth landing site were shown by the Apollo missions where man performed the surface sensing and steering functions. Apollo 11 required a last second maneuver by Neil Armstrong to avoid a boulder field that lay in the targeted area. For unmanned missions, an autonomous real-time surface sensing system is desirable to enable safe targeting to geologically interesting landing sites on distant planets. The need is further dramatized by the failures of the Russian Mars landers and the more recent Luna 23 that was damaged on impact. The feasibility of such a system has been studied and the results are reported here.

The Viking Mars mission was used in this study to arrive at a consistent and realistic set of design requirements and goals. The system must be compatible with the Viking lander in terms of mission profile, vehicle dynamics, interfacing, and environmental requirements. It also must be able to detect and avoid 22-cm obstacles during the latter portion of the terminal descent phase; therefore, a TV imaging system with contrast avoidance logic was chosen for the reference configuration.

The primary objective of this study was to design and test a breadboarded video guidance system that would demonstrate the capability to autonomously select the least hazardous landing site on a scaled three-dimensional planetary surface model. This was accomplished by a coordinated physical and digital simulation effort that established system feasibility.

The approach taken was to (1) establish the reference mission requirements, constraints, and maneuver capability, (2) breadboard the video data processing logic and integrate it with an image dissector camera, (3) design and build a physical simulator, (4) integrate and program the PDP-9 scientific computer to drive the physical simulator to simulate flights to the surface, (5) build a scaled three-dimensional Mars surface model to be used as the target, (6) check out and calibrate the total integrated system, and (7) run a Monte Carlo simulation consisting of repeated flights to the surface from arbitrary starting positions and altitudes.

Feasibility was based on the system's ability to repeatedly locate the most acceptable landing site in arbitrary areas regardless of initial conditions.

The following guidelines were used in performance of this study:

- 1) The lander vehicle and flight characteristics were assumed to be similar to those of the '75 Viking vehicle;
- 2) A median atmospheric density profile exists at terminal descent altitudes;
- 3) The lander propulsion system may have up to 10 kg of propellant available for site selection maneuvers;
- 4) The Mars terrain model shall have several hazardous regions and several "safe" landing sites;
- 5) The color and texture of the terrain surface and its illumination should be chosen to represent nominal surface conditions, not extreme conditions.

The techniques employed, hardware and software implemented, physical simulator characteristics, and experimental results are documented and discussed in this report. However, it should be noted that no attempt was made to optimize the VGLIS hardware for the Viking lander application because that is beyond the scope of this study.

The contents of this report is organized in the following manner: the Summary section summarizes the results of the feasibility demonstration and includes the study recommendations.

As a point of reference, the Introduction describes the main objectives, the study approach, and guidelines.

The System Operation section is as implied and also contains a description of the physical simulator and scaled Mars surface model.

The Surface Model section contains a summary of the ingredients that went into construction of the three-dimensional target.

The Experimental Results section describes the experimental procedure, calibration technique, algorithm evaluation experiments, and the Monte Carlo simulation activity used in establishing system feasibility.

The Mission Considerations section summarizes the Mars mission and Viking lander constraints and the maneuver capability study results.

The Hardware and Interface Requirements section was added to provide an approximate weight and power estimate for an eventual flight system.

The last section, Recommendations, is included to suggest a cost-effective approach to the further development and use of the VGLIS technology. The simplicity of design and added scientific utilization of this technology make it particularly applicable to advanced planetary programs.

SYSTEM OPERATION

Flight System

The video guidance, landing, and imaging system (VGLIS) is a unique approach to increasing the probability of a successful landing on an unknown surface. It will therefore significantly contribute to the adaptive capability of the lander. It consists of a TV camera as the sensor and the processing electronics that operates on the raw video data and outputs a steering bias to the lander computer. The uniqueness of this approach is in the video signal processing logic, which is simple in design and makes maximum use of the available data.

The VGLIS is especially applicable to a planetary lander mission in which the detailed surface feature characteristics are not known before the landing. For the Viking mission, the system would be turned on after having jettisoned the parachute and would continue to operate as it approaches the planet's surface as shown in figure 2. At approximately 900 meters the system is activated and dynamically scans the area surrounding the predicted impact point (PIP) as determined by the lander computer. The video data are then processed, resulting in a steering command to the lander computer and, consequently, to the propulsion subsystem to avoid rocks, craters, and major slopes as shown in figure 3. The PIP is always within the 60 x 60-degree total field of view (TFOV). The 60-degree TFOV is necessary to permit observing the PIP in spite of anticipated vehicle attitude excursions necessary for maneuvering during the terminal landing phase. Use of electronic beam positioning obviates the need for extensive data processing of the entire area, for mechanical gimbals, and for reorienting the vehicle to observe the area about the PIP. The scanned field of view diminishes as a function of altitude while resolution improves.

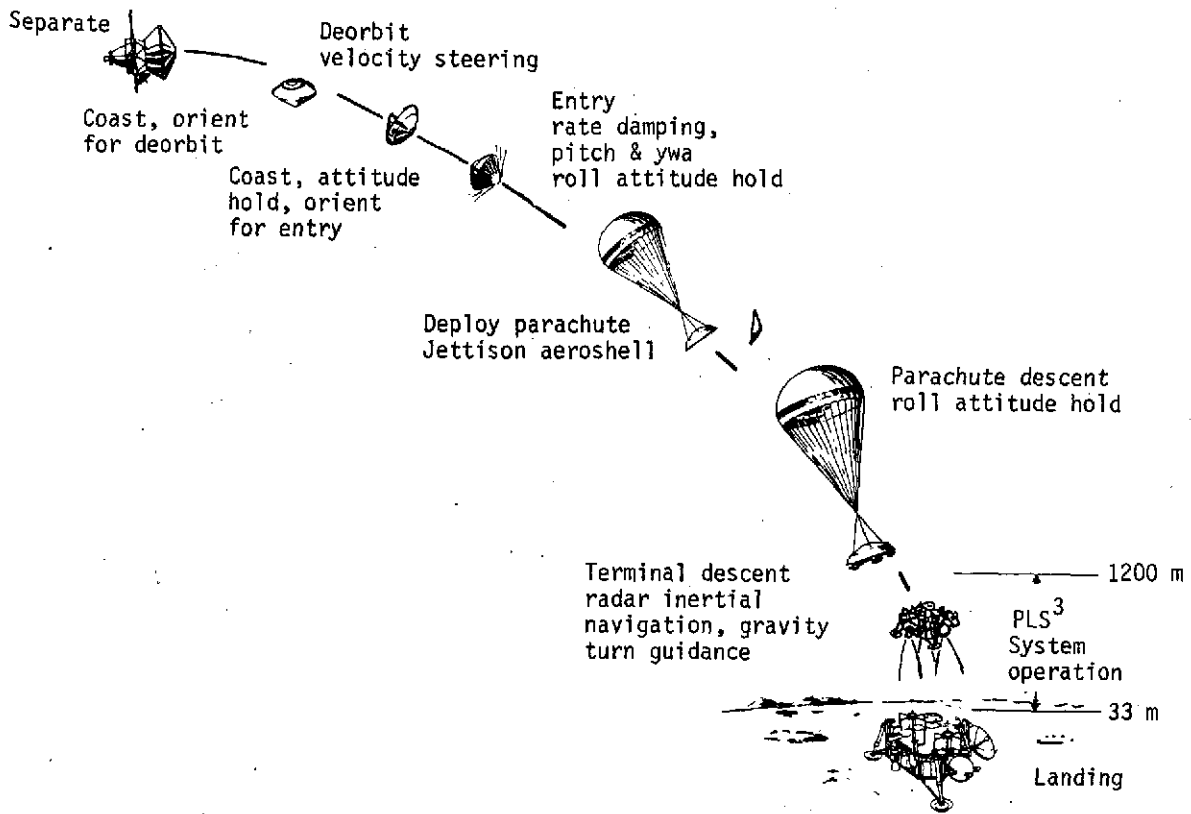


Figure 2.- Reference Mission - Viking

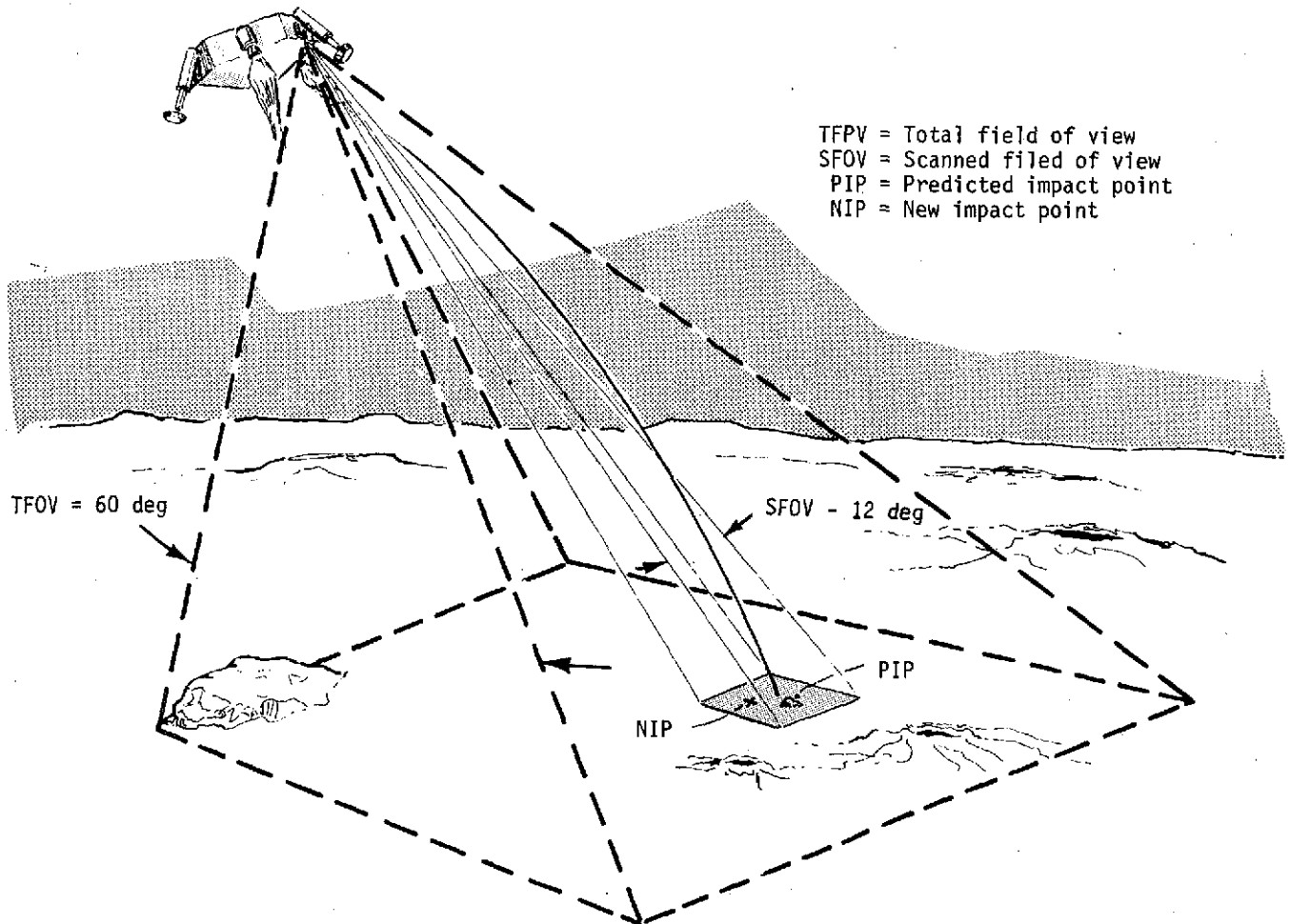


Figure 3.- System Operation

After the VGLIS scans the surface, the video data are processed and a new impact point is selected (the area with the least contrast). A bias steering command to the lander computer enables maneuvering to the preferred landing site. The sequence is repeated at 1-second intervals down to approximately 33 meters from the surface. Operating time varies from 20 to 35 seconds as a function of wind velocity, atmospheric density, and maneuver distance.

Laboratory System

Overview. - The VGLIS simulator hardware is described in detail in the paragraphs to follow. This subsection contains a description of the physical layout of the simulator, and the remainder of the section deals with the functional characteristics.

Based on physical location, the VGLIS simulator may be divided in four major subsystems--the simulator carriage, the control console, the computer, and the surface model. The surface model is discussed in the next section.

Figure 4 (6-D simulator) shows the simulator carriage. The long horizontal boom moves along the vertical tracks at each end. This degree of freedom is defined to be the Z axis. The smaller horizontal boom moves left and right along the larger boom for the + X motion. A third assembly moves along the small boom to provide the third degree of freedom, + Y. The camera head and the motorized lens are attached to this assembly and mounted vertically. The camera head and lens are about equal in length. A three-axis attitude gimbal is also available but was not used in this study. The camera electronics module is not shown. The entire carriage is precisely counterweighted to offset any biased load on the Z-axis motors. The counterweights can be seen at the lower center of the photo.

Figure 5 depicts the control console, which is situated on an elevated platform in the same laboratory as the simulator carriage. The center console section is the monitor. On the right are the control panel and a digital voltmeter used for various monitoring functions. The control panel includes the manual controls for the carriage and lens, the master and servo power controls, and the switches that control whether operation is in the manual or automated mode. The power supplies and camera control unit are below the desk surface of the console. To the right of the console is the teletype used for computer input.

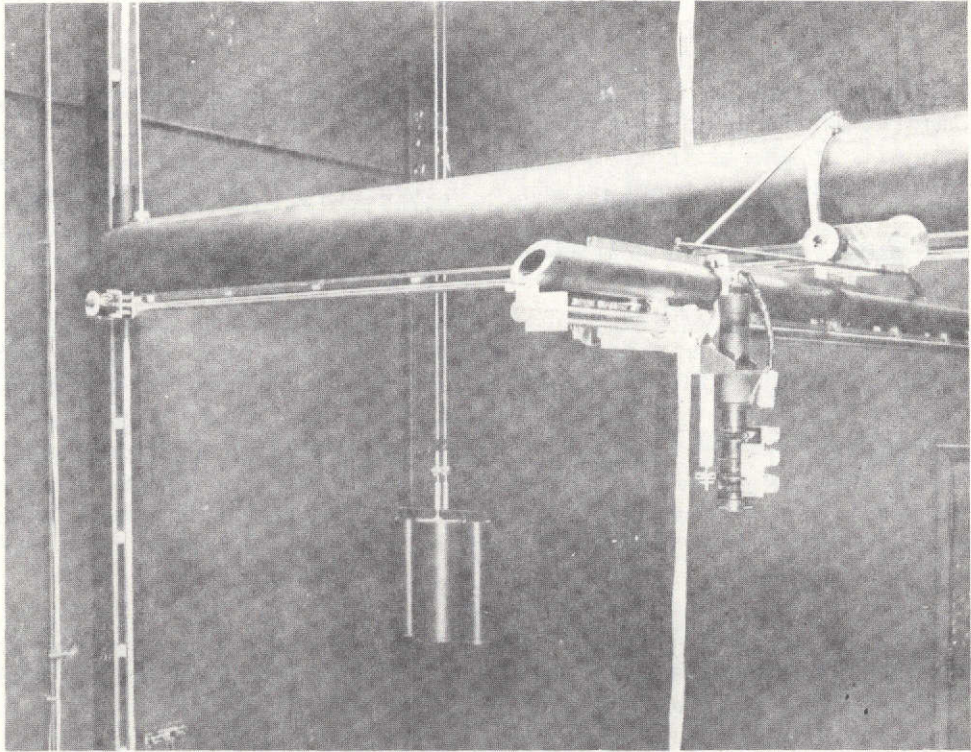


Figure 4.- 6-D Simulator

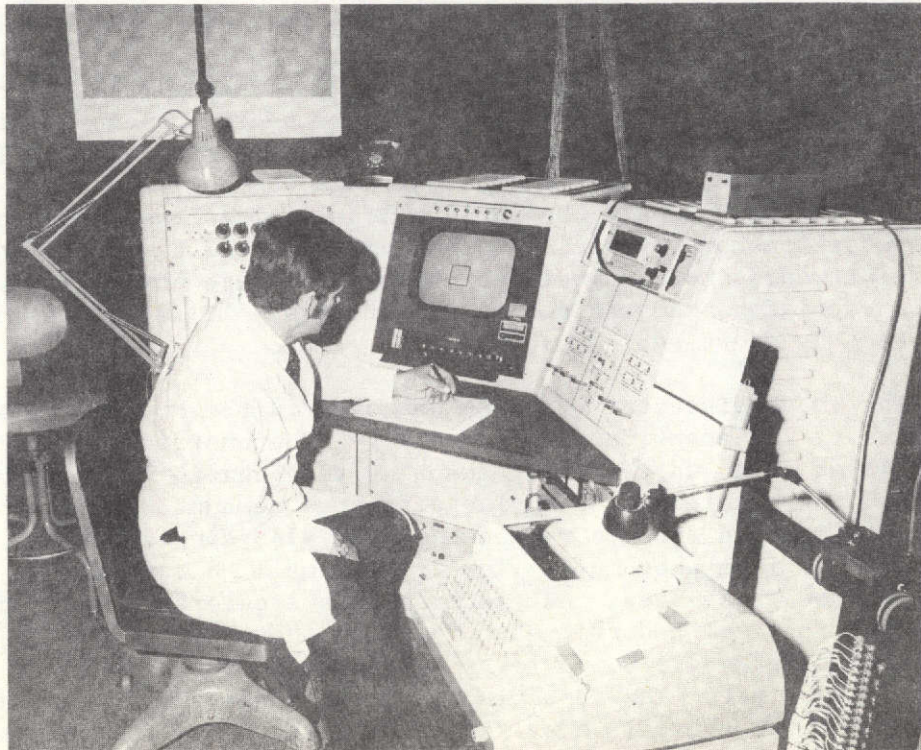


Figure 5.- Control Console

Figure 6 shows the Digital Equipment Corporation PDP-9 digital computer. The computer is the large unit on the right. The smaller unit at the left is the printer. Servosystem commands are generated by the computer after analyzing the three processed video signals. The interaction between the console and the computer also determines where the camera and monitor beams can sweep.

The preceding discussion treated the system as comprising four separate physical entities. Because the remainder of this section will be devoted to the operational characteristics, the subsystems must be regrouped in a more functional association regardless of their physical location. These functional groupings are (1) the camera control system, (2) the video processor, (3) the simulator translational servosystem, and (4) the computer interface. During the discussion to follow, it will be helpful to refer to figure 7, the VGLIS simulator functional block diagram.

Camera Control System. - The image dissector camera system consists of a camera with servo-controlled lens, a monitor and a digital sweep generator (fig. 7). The system allows for remote control of the following parameters--iris, focus, zoom, and field-of-view segment.

Three parts of the camera system are located on the simulator carriage--the head, the lens, and the electronics module. The head is a cylindrical tube containing the vidicon, deflection coils, and a video preamplifier. The servo-driven lens is attached to the front of the head along the same axial line. This assembly is then oriented on the carriage so the lens points vertically downward toward the surface model. The lens also contains the dc servomotors, position potentiometers, and associated gearing. The electronics module includes the high-voltage power supply, the focus regulator, and the deflection drivers. It is connected to the head by short cables.

The image dissector (fig. 8) was used in the breadboard system because of its adaptive sensing ability, photometric output, and controlled scan, which permit adapting to a change in scan position or lighting conditions on an instantaneous demand. Its immunity to sterilization and its ruggedness were also considerations. Basically, it is a photomultiplier with a small, electronically movable photocathode area. An electron lens accelerates and focuses all electrons emitted from each point on the photocathode to a corresponding single point (or small area) in the plane of a dissecting aperture. The resulting electron image, which is a direct measure of the optical input radiation pattern, is then electronically deflected across the aperture. The aperture consequently

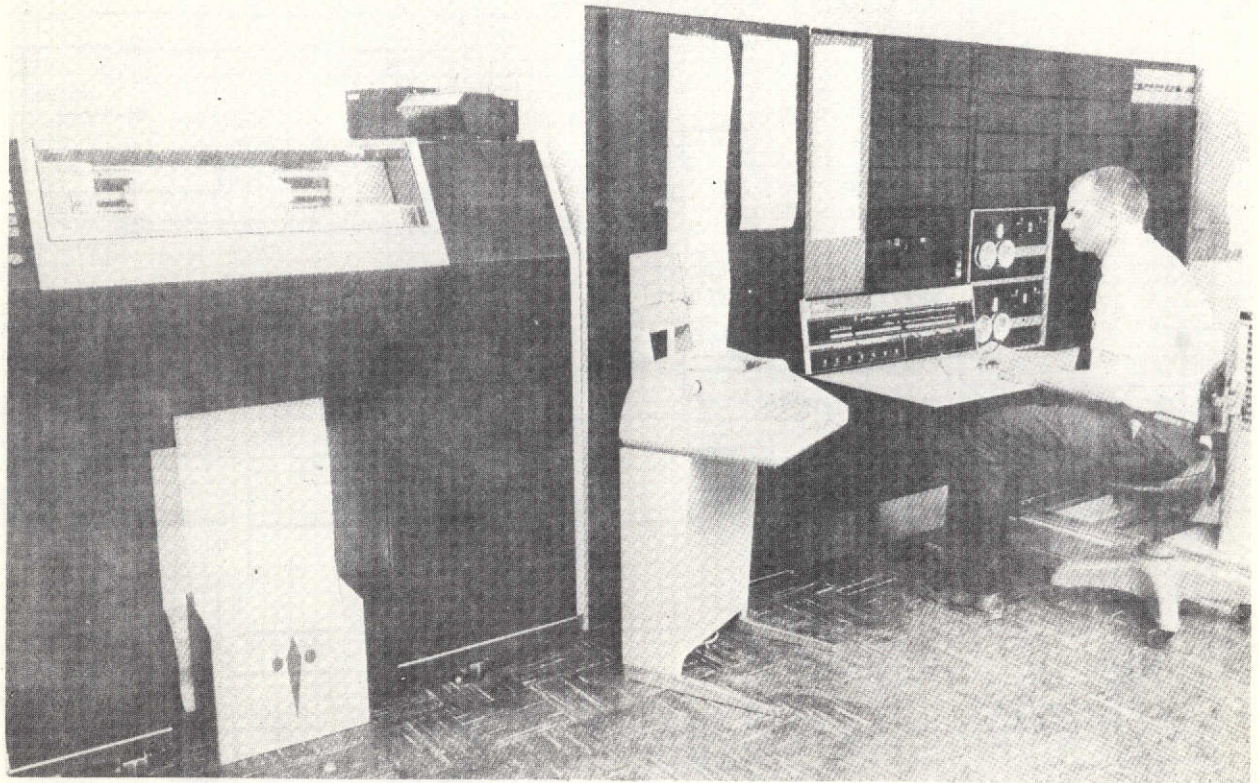


Figure 6.- PDP-9 Digital Computer

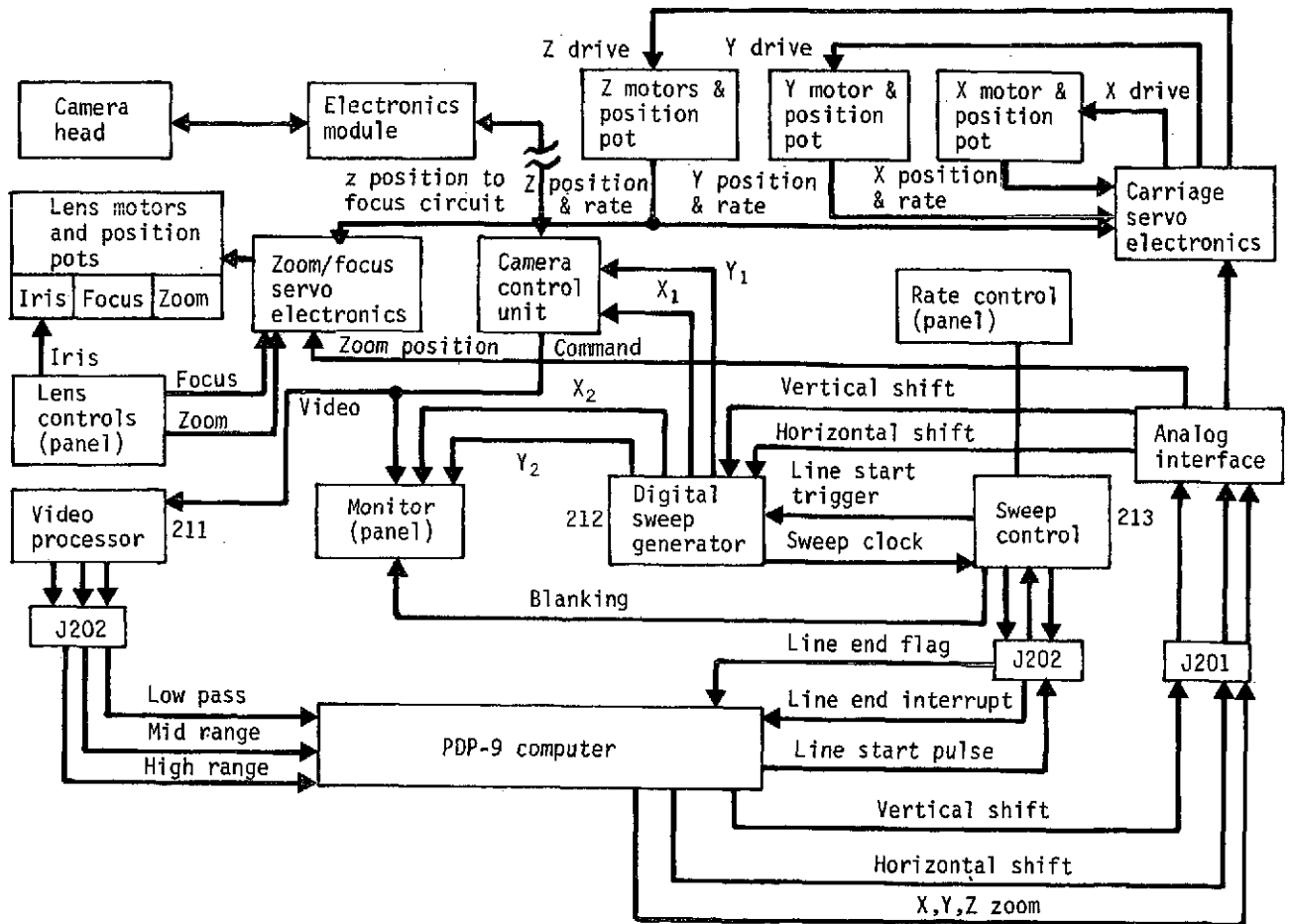


Figure 7.- VGLIS Simulator Functional Block Diagram

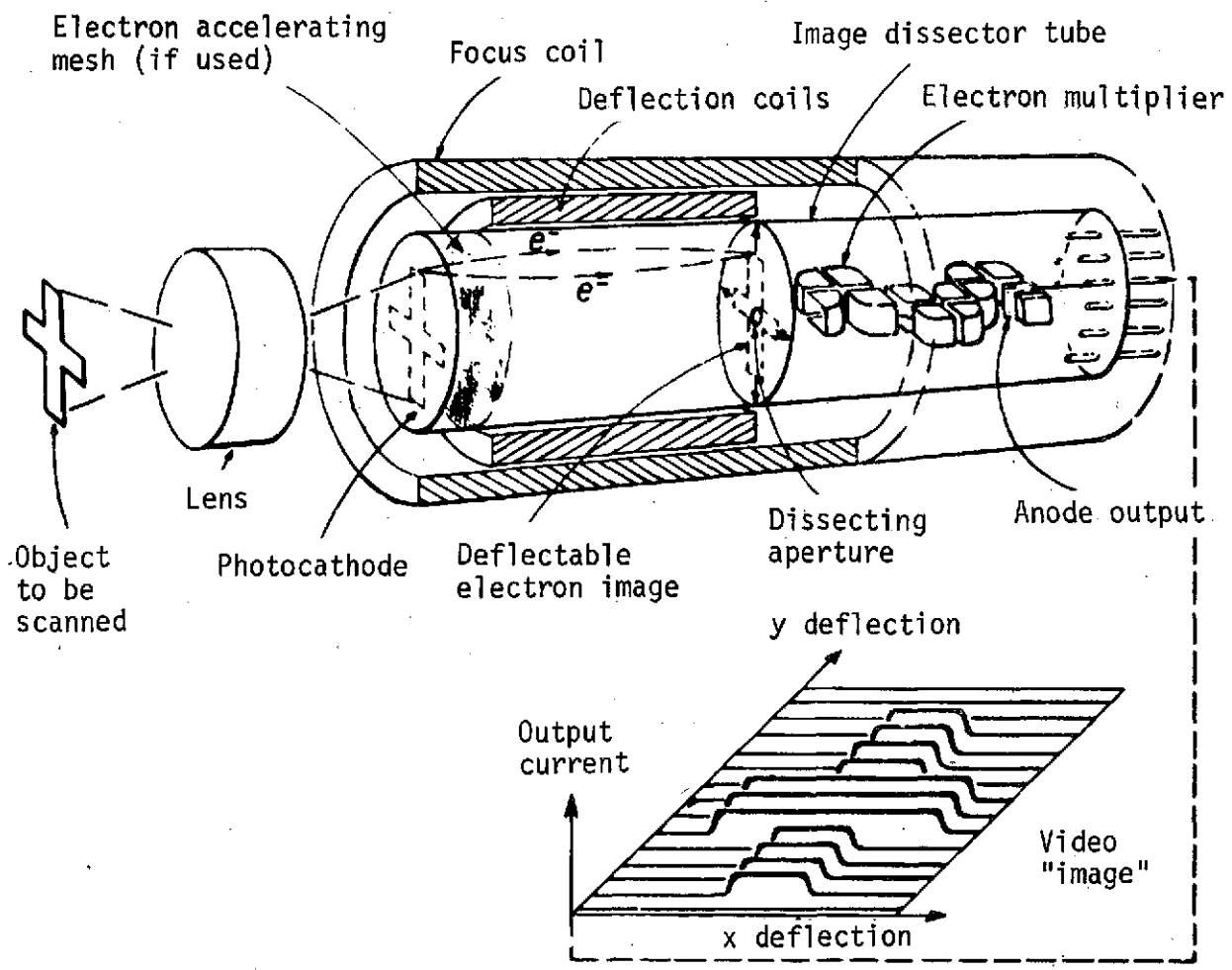


Figure 8.- Image Dissector

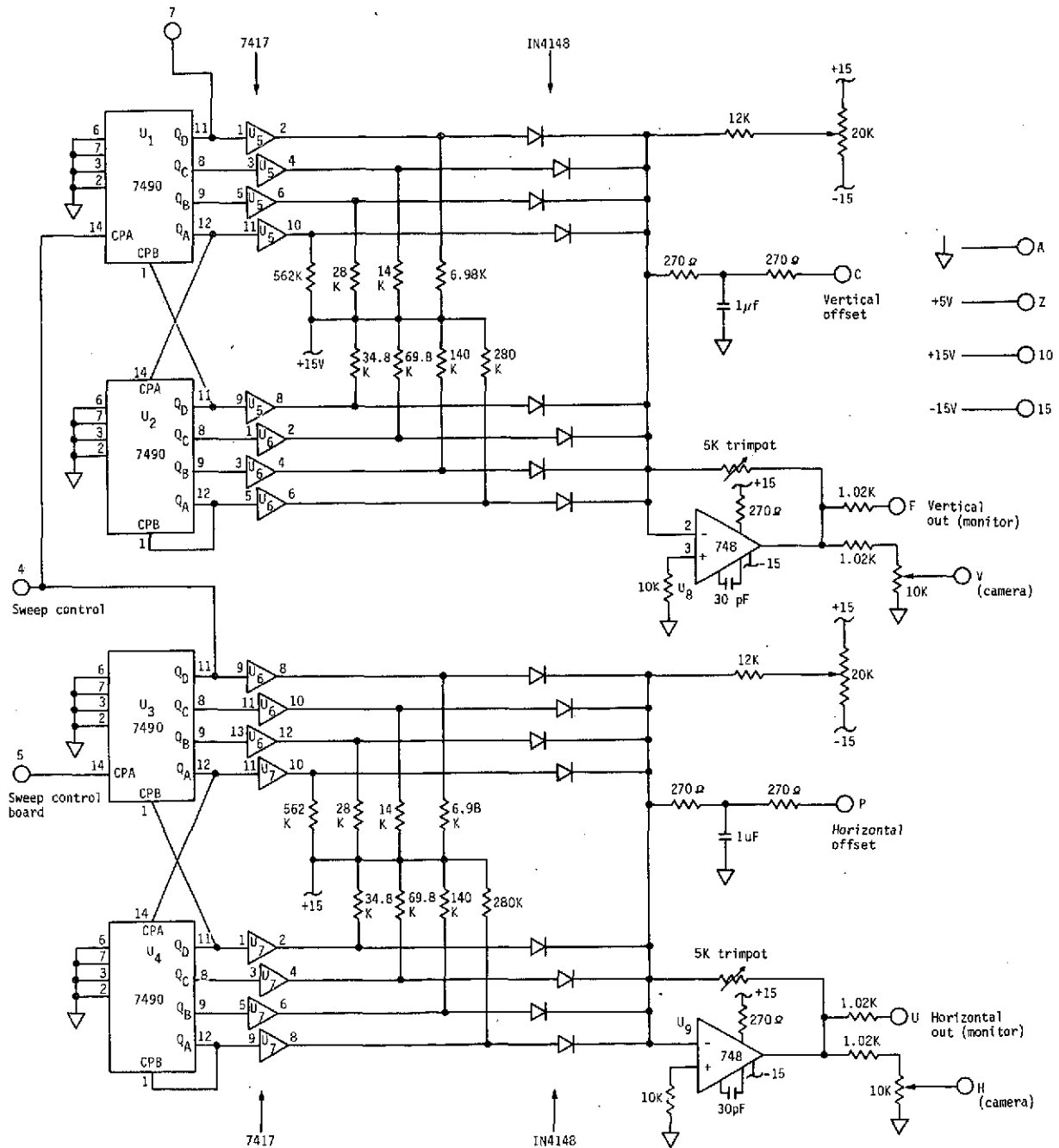


Figure 9.- Digital Sweep Circuit

The lens control system allows remote operation of iris, focus, and zoom. The iris control is simply a manually operated front panel switch on the control console. No provision is made--or is necessary--for automatic iris operation. Zoom and focus are controlled by very similar dc servosystems. Both contain a diode function generator to match the lens characteristics to a linear input command. Zoom can respond either to a manual input or to a computer-generated "altitude" signal. Focus is normally under control of the Z-axis (vertical) position potentiometer so the scene remains in focus regardless of the vertical displacement. Focus may also be varied manually. The lens servosystems are simple position-loop dc servos with a hybrid integrated circuit power amplifier. The amplifiers are provided with electrical limits to prevent driving the lens beyond its normal end points.

Video Signal Processing

As the lander enters its final descent phase, the on-board navigation computer starts the system and sends it positioning information. Based on this information, the system television camera scans several areas on its photocathode centered around the image of the predicted impact point. The system processes the video signal from the camera to get a "site suitability rating" for each of the areas. After the areas have been scanned, the system sends digital signals to the navigation computer telling it which area was best, and the computer maneuvers the lander toward the corresponding site on the ground. The system then receives positioning information for a new predicted impact point, and the process continues until either the fuel allotted for maneuvering is consumed, or the lander reaches an altitude of 33 meters below which further maneuvering is not desirable.

The suitability ratings are based on picture contrast because rugged areas tend to produce pictures with greater contrast than smooth areas. A simple index of contrast in a video signal is the ratio of an average ac component in the signal to an average dc component. In practice, it may be desirable to use several filters to find the ac components in each of several bands.

In the laboratory version of the system, a linear response image dissector television camera was attached to a computer-controlled simulator with three translational degrees of freedom and suspended over a 50-square-foot octagonal "sandbox" surface model. The computer controls camera position with respect to the model and the zoom lens focal length and focusing by sending analog signals from digital-to-analog converters to servos. Because the

samples, at any instant of time, the photocathode. Following the aperture, the sampled photoelectrons are multiplied in an electron multiplier by a large factor (commonly 10^5 or 10^7), and emerge as a current in the output anode circuit. Therefore, the detector output is a direct function of the light flux incident on the photocathode (image plane), and hence is a direct function of the illumination from the projected sample area on the surface.

The remainder of the camera system is located in the control console. The monitor has the standard array of controls--e.g., brightness, contrast, focus, etc--and in addition has an X-Y deflection capability to permit external sweep voltages to be applied. The control console also contains the camera dc power supplies, the lens servo electronics, and the digital sweep circuits.

The digital sweep circuit shown in figure 9 provides horizontal and vertical sweep signals for both camera and monitor. A 100-kHz square wave from the sweep clock is introduced at pin 14 or U3. Counters U3 and U4 are divide-by-10 counters with a binary-coded-decimal (BCD) output that steps from 0 to 99 before resetting. The BCD outputs are buffered by U6 and U7. As each output of U6 and U7 goes high according to the BCD code, current from its associated resistor flows into the summing junction of U9, an operational amplifier. This process produces a digital-to-analog (D/A) conversion and the output of U9 is an analog sweep with only about 1% deviation from linearity. An offset signal can be applied through two 270-ohm resistors to control the placement of the raster in the horizontal direction. In the current simulation this input is under computer control and used to select the segment of the field of view to be analyzed. An output from counter U3 is sent to the sweep control circuit to signal the completion of one horizontal line. At the end of each line the sweep is stopped while the computer analyzes the data from that line and then signals the sweep control circuit to sweep another horizontal line. The vertical sweep circuit is identical to the horizontal sweep except that counters U1 and U2 step one count for each horizontal line. The vertical sweep therefore consists of 100 horizontal lines. With a sweep oscillator frequency of 100 kHz, a frame is completed each 1/10 second (10 frames/second). At the end of each frame an output from U1 signals the computer for synchronization purposes. In both the horizontal and vertical sweep circuits, a separate gain control is provided for the camera. The sweep control circuit is covered as part of the computer interface discussion.

vertical camera motion was restricted by the minimum focusing distance and the height of the room, it was necessary to vary the zoom lens focal length to simulate altitude. The same restrictions made it necessary for the computer to physically center the camera over each predicted impact point rather than simply bias the scanning as would be done on a flight version of the system.

Nine square area subframes in a 3x3 square matrix were evaluated for each guidance decision. Scanning signals were biased to move the scanned area on the photocathode to each of the nine areas in turn. Each of the subframes was scanned once requiring 0.1 second per frame with 100 lines per subframe, 100 picture elements per line. This produced approximately one guidance decision per second. Since landing time for the Viking lander is expected to be on the order of 20 to 30 seconds, 20 guidance decisions per landing were used in the experiments.

The video signal was processed by the circuit in figure 10. In this circuit, U1 and associated circuitry form a 30-kHz low-pass filter to remove noise at frequencies above the resolution limit of the camera. The output of this filter goes to U2, U4, and U7. Counter U2 is a 20-Hz low-pass filter, and its output ($-V_L$) is proportional to the dc component of the video signal. This signal is inverted by U3 for compatibility with the computer A/D converter. Counter U4 is a high-pass filter. It extracts the 1-through 30-kHz portion of the video signal. Counter U7 is a band-pass filter to extract the 30-Hz through 9-kHz portion of the signal. Direct current voltages (V_H and V_M) proportional to these ac components are produced by full-wave rectifiers and smoothing filters composed of U5, U6, U7, and U8. The three signals to the computer, V_L , V_H , and V_M , then represent the rectified integral of the dc component, the high-frequency ac components, and the low to middle frequency ac components of the video signal, respectively. The computer then sensed and performed A/D conversion on these signals at the end of each line and averaged the lines digitally. This allowed smoothing filter time constants to be short so each of the nine subframes would need to be scanned only once. (The same result could be achieved in a flight version by using resettable integrators instead of smoothing filters and sampling and resetting once per subframe. However, the technique used in the breadboard system allowed great flexibility for experimentation.)

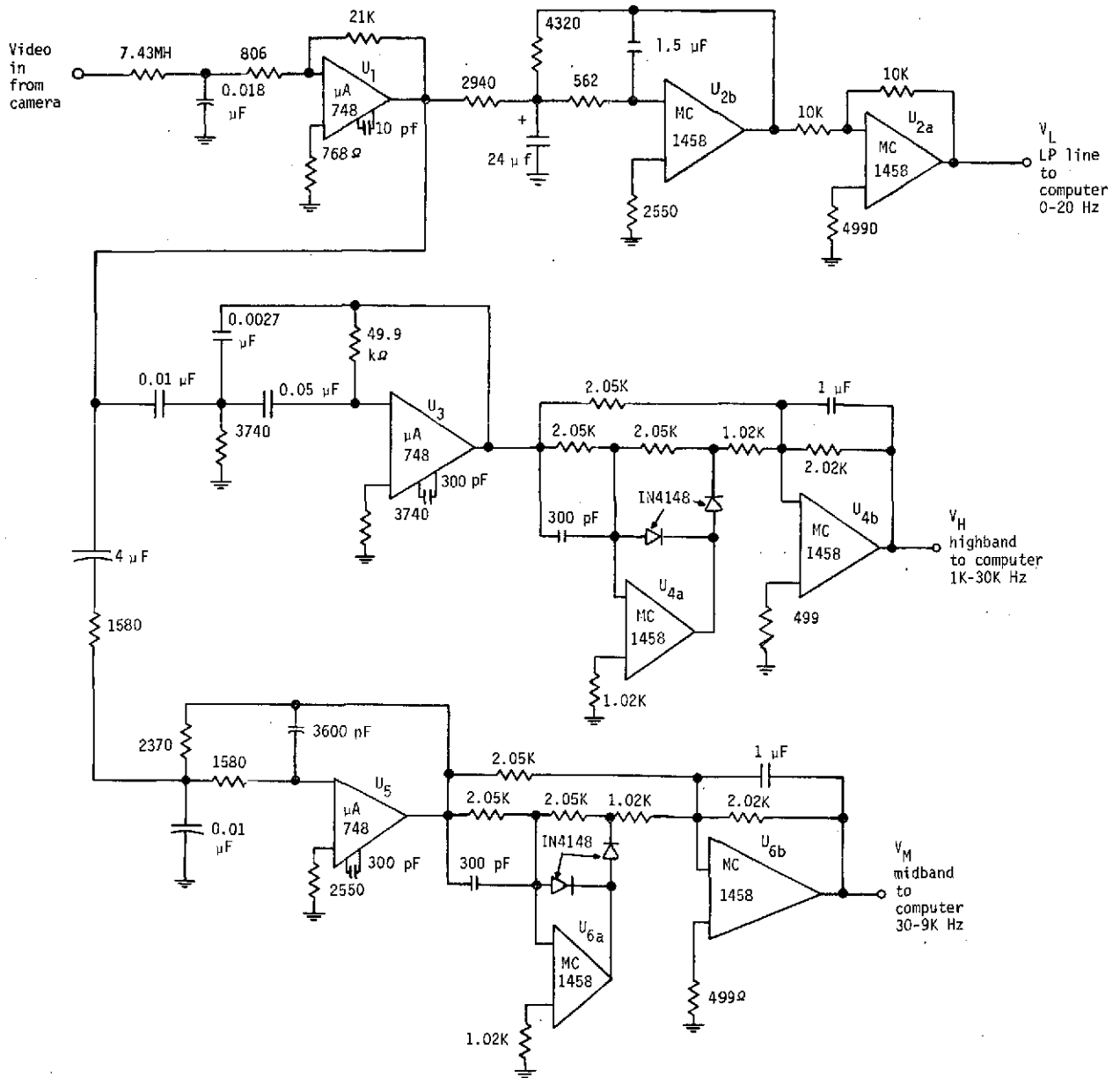


Figure 10.- Video Signal Processor

The computer was used to calculate the "suitability rating" for each subframe so different rating schemes could be implemented quickly. This function, however, could be performed by dedicated circuitry in a flight version. The rating scheme used was

$$\text{Rating} = a \left(\frac{|\bar{V}_M| - b}{|\bar{V}_L| - c} \right) + \left(\frac{|\bar{V}_H| - d}{|\bar{V}_L| - e} \right)$$

where $|\bar{V}_M|$, $|\bar{V}_H|$, and $|\bar{V}_L|$ are the absolute values of the average values of V_M , V_H , and V_L for a subframe, and the constants b , c , d , and e are determined experimentally to correct for amplifier offset voltages and noise, making the rating nearly independent of lighting intensity. The weighting factor "a" was selected empirically to give best agreement between the algorithm and the experimenter's subjective evaluation of various areas. (Because V_M is approximately proportional to V_H , the rating does not greatly depend on the value of "a" for typical surface areas, and experimental results suggest that there may be little or no advantage in using two ac outputs instead of one. Use of both V_M and V_H in the breadboard system, however, allowed for greater flexibility in experimentation.) In the feasibility tests, the following values were used for these constants-- $a = 0.6$, $b = 0.1$, $c = 0.62$, $d = 0.95$, $e = 1.7$. The factors b , c , d , and e might be eliminated in a flight version of the system because the noise and offsets become less significant when the light intensity is increased. Changing from a spotlight to sunlight would have this effect.

The computer compared the ratings of the nine subframes and selected the one with the lowest rating. (In a flight version of the system this function could also be performed by dedicated hardware to minimize impact on the navigation computer.) Having selected this as the best area, it solved equations to determine the new predicted impact point and new altitude, and the process was repeated until the simulated altitude reached 33 meters.

Simulator Translational Servosystem. - The simulator carriage, as employed in the current simulations, has three degrees of freedom--Z (up/down), X (fore/aft), and Y (port/starboard). Each axis is remotely operated either manually or by computer command. The X and Y axes are each moved by a single dc servomotor while the large boom is moved in the $\pm Z$ directions by two servomotors,

one at each end. Each axis has a position loop served by a single position potentiometer and a rate loop, for improved stability, is provided by a tachometer. The computer inputs are position commands, and the manual inputs command a rate. The Z axis can maneuver the camera image plane between 1.52 and 3.35 meters from the model surface. The X and Y axes have sufficient range to cover all parts of the surface.

Computer Interface. - The computer interface circuits include all the analog signal conditioning and digital sequencing required to transfer data and commands between the PDP-9 and the simulator control console. The interface electronics is divided into the sweep control circuit, the analog interface circuit, and the video processor circuit (fig. 10).

The video processor, discussed elsewhere in this report, provides three outputs--low, medium, and high frequency bands. The output amplifiers on this circuit card translate these signals to a range of from 0 to -10 volts for compatibility with the PDP-9 A/D converter inputs.

The analog interface circuits are an array of differential amplifiers designed to provide unity gain to the analog command signals from the computer, yet reject any common-mode noise that may be present. The outputs of these amplifiers are the position commands to the simulator servoamplifiers and to the horizontal and vertical sweep generator offsets.

The sweep control circuit provides the sweep clock signal and serves as the interface between the camera control system and the computer. The sweep clock--as mentioned earlier--runs at a nominal frequency of 100 kHz for a 10-frames per second rate. The oscillator frequency can be varied over an 8 to 1 range by a panel control. The oscillator output passes through a gate to the digital sweep circuit. When the gate is open, the oscillator signal causes the digital sweep circuit to produce one horizontal line. At the end of a line the gate closes and an interrupt signal is sent to the computer. This signal tells the computer that the video processor has data waiting. When the computer acknowledges and converts the video data, it sends a pulse to the sweep control circuit. This pulse opens the gate and allows the system to scan another line. The process is repeated over and over until the vertical sync signal from the digital sweep board arrives at the sweep control board. The leading edge of the vertical sync signal sets a flip-flop. The flip-flop output is translated to a negative voltage by an operational amplifier and is sent to the computer as an

analog input. The computer checks for the presence of this signal at the end of each horizontal line. When it is received it is interpreted as the end of a frame. The computer reacts by changing the offsets to scan a new area or by analyzing the data if the area scanned was the final area of the series. As shown in figure 11, nine nonoverlapping areas are scanned with the deflection offsets changed between each area or frame. The computer then determines the smoothest frame of the nine-frame series. The digital signals in both directions between the sweep control circuit and the computer are conditioned by line drivers and receivers for improved noise immunity. One other output from the sweep control board is used to blank the monitor when the sweep is not moving, thus preventing the stationary beam from burning the phosphor.

SURFACE MODEL

The surface simulation model used in the feasibility demonstration consisted of a 2.44-meter diameter octagonal box filled with 10.16 centimeters of lunar nominal NASA-furnished material, as shown in figure 12. Surface morphology variations were implemented via the formation of craters, channels and channel outlets, volcanic structures, dunes, ripples, and knolls. Multiple variations in surface granularity were accomplished by screening the model material to control obstacle distribution and to effect albedo variations. Subsequent sessions with members of the Viking Site Certification Group resulted in further refinements to the surface model. An attempt was made by Dr. H. Masursky *et al.* to arrive at earth analogies of Martian features such as might be found in the dry valleys of South Victoria Land, Antarctica, or in the coastal desert of Peru. As an example, six of the seven types of wind erosional land forms recognized on Mars are present in the Peruvian desert. Also, the clearly aeolian light and dark plumes on Mars have Peruvian counterparts. The morphology of the Martian dunes resembles that found in Peru. It has been inferred that both small- and large-scale sand and possibly granule ripples also exist on the surface of Mars but were not seen because they were below the limit of the Mariner 9 cameras. Dark lag gravels or desert pavements are also almost surely present.* Selected photographs of areas of interest are shown in figure 13.

* Grollier, M. J., Ericksen, G. E., McCauley, J. F., and Morris, E. C., "The Desert Land Forms of Peru: A Preliminary Photographic Atlas." U. S. Department of the Interior Geological Survey, Interagency Report, Astrogeology 57, February 1972.

No overlap
between areas

H = -1.43 V = +1.43 A11	H = 0 V = +1.43 A12	H = +1.43 V = +1.43 A13
H = -1.43 V = 0 A21	H = 0 V = 0 A22	H = +1.43 V = 0 A23
H = -1.43 V = 1.43 A31	H = 0 V = -1.43 A32	H = +1.43 V = -1.43 A33

H = Horizontal offset voltage
V = Vertical offset voltage

Figure 11.- Scan Layout

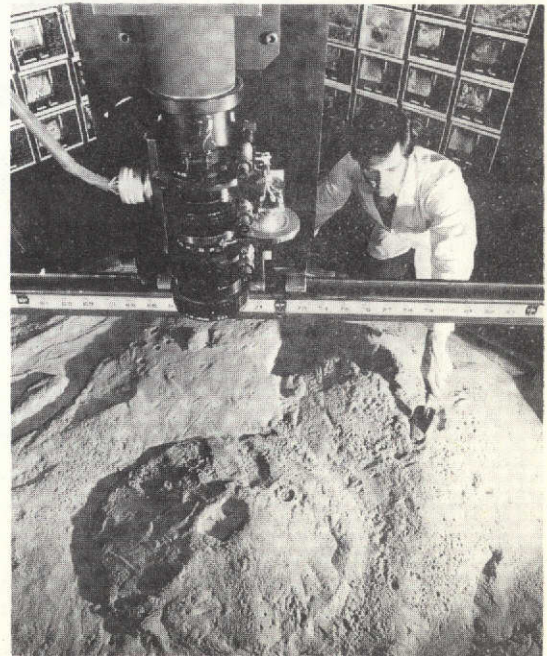
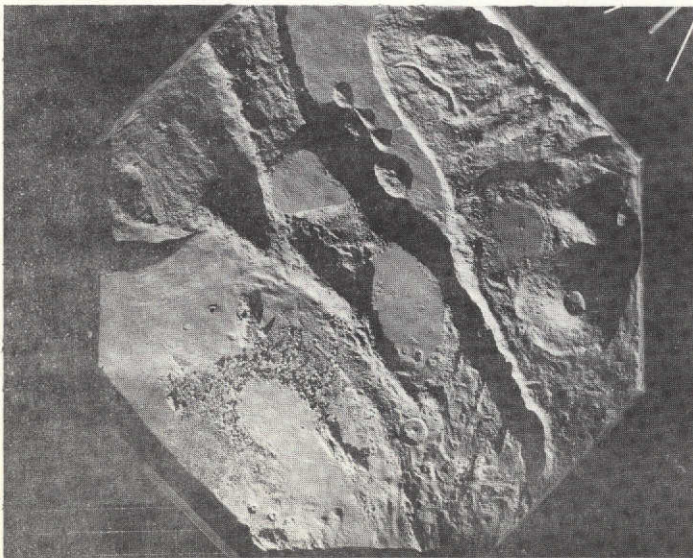


Figure 12.- Surface Simulation Model



Figure 13.- Desert Land Forms of Peru

Still other Martian analogies can be made to the Dry Valleys of South Victoria Land, Antarctica. Implications for a Viking type lander are as stated by Morris, Mutch, and Holt.*

"Various features seen in the Dry Valleys may be similar to features that might be encountered on Mars. Having some understanding of this terrestrial cold desert region, our capability for prediction and interpretation is increased. Some examples are as follows:

- 1) Cavernous weathering of boulders produces strange forms that, in low-resolution photographs, could easily be taken for artifacts or biologic forms;
- 2) Cavernous weathering characterizes a cold, windy environment, but similar erosional forms can be produced in a variety of terrestrial environments;
- 3) Ventifacts can be formed in brief periods of time--months to decades. Orientation of facets provides a record of prevailing wind direction;
- 4) Erosional and depositional features in the vicinity of boulders provide a record of recent wind direction;
- 5) Cavernous weathering occurs in coarse-grained rocks. Fine-grained rocks form classical ventifacts;
- 6) Winds in the vicinity of 200 km/hr can form pebble ridges;
- 7) Armored pavements of coarse fragments, formed by deflation of fine materials, are common in the Dry Valleys and in many other desert regions. The pavement can be easily penetrated to obtain underlying finer sediment;
- 8) Antarctic soils are very poorly sorted with a marked deficiency of fine clay material relative to most other terrestrial soils and sediments;

* Morris, E. C., Mutch, T. A., and Holt, H. E., "Atlas of Geologic Features in the Dry Valleys of South Victoria Land, Antarctica." U. S. Department of the Interior Geological Survey, Interagency Report, Astrogeology 52, September 1972.

- 9) Physical disaggregation of rocks to produce the forms observed in the Dry Valleys probably involves frost shattering;
- 10) Patterned ground is produced when an ice layer is situated within several meters of the surface;
- 11) The size of ice wedges and the amount of ground deformation adjacent to them is related to their age;
- 12) Moist soil overlies permafrost, even though little or no moisture is derived from the atmosphere;
- 13) Concentrations of salts occur throughout the soil in this cold desert region;
- 14) The geochemical significance of the salts is difficult to establish;
- 15) Weathering of bedrock involves little chemical modification;
- 16) Interbedded aeolian sand and snow produce lithified strata that closely resemble more common bedded sedimentary rocks;
- 17) Sand dunes accumulating when temperatures are slightly below freezing are characterized by snow-sand cornices building out over the lee slopes of dunes;
- 18) Most of the large boulders observed throughout the Dry Valleys have been transported to their present sites by glaciers. (There is no evidence for a similar transportational environment on Mars, at least in the Viking zone of interest.)"

EXPERIMENTAL RESULTS

This section summarizes the calibration technique and experimental data resulting from multiple flights to the surface via the laboratory system described in the preceding section.

The optical calibration phase consisted of two series of experiments designed to characterize actual system performance. These experiments resulted in an estimate of video system performance, i.e., a measure of the system's ability to "see" a given target.

The "experimental results," as discussed in this section, provide the basis for the feasibility demonstration by applying statistical analysis, i.e., a Monte Carlo approach, to the "flight" results. This provided a quantitative basis for evaluation of performance capability.

Calibration

Camera System Performance. - Because the system logic is essentially based on contrast avoidance, or more specifically on avoiding terrain containing relatively larger amounts of spectral power at higher frequencies, the transfer of signal modulation through the system is of primary importance. There are a number of elements that can affect the overall modulation transfer function (MTF).

The modulation transfer function, as applied to the VGLIS, is a curve that shows the modulation transfer of the system or one of its components (lens, imaging tube, electronic circuits, or complete system) as a function of the spatial frequency of information in the scene viewed by the camera. The modulation transfer for any specific spatial frequency is determined by viewing a target that is produced and calibrated to present a known contrast at that spatial frequency. The modulation transfer for that frequency is then the ratio between the contrast indicated by the system's or component's output and the known contrast of the target.

Several of the elements that affect the MTF are as follows:

- 1) Zoom lens - The performance of the laboratory system compared to what could be achieved in the flight situation is considerably degraded by the necessity to employ

the servo-controlled zoom lens. Such a lens can truly be said to possess an infinitely large family of MTFs that depend on the zoom focal length, position in the field, and object distance. Aperture vignetting is also a problem that varies with focal length. Finally, there are practical problems in precisely mounting the lens on the camera so an optimum focus exists over the full range of focal lengths, and then to correctly adjust the analog function generator to maintain focus as the camera moves up and down;

- 2) Camera - The MTF performance of the image dissector camera is primarily governed by the size and shape of the scanning aperture, with the electron optics being a secondary influence. Although the MTF of the camera also varies with radial position off-axis, in the present case the maximum radial offset is only about 60% of the capability of the tube so this variation is minor;
- 3) Signal processing electronics - Video signal amplification by the image dissector multiplier section is very broad-band, as are the current-to-voltage and line-driving voltage-follower amplifiers contained in the camera assembly. The MTFs of these stages can be ignored. Each spectral band of the contrast avoidance logic will, of course, be represented by a different MTF, but as far as the signal delivered to the logic is concerned, the rolloff of the initial low-pass filter is the dominant factor electrically.

The influence of the above factors is shown in figure 14. Because all of the experimental work in this phase of the program was performed at an optical object distance of about 3.35 meters, the scale of the abscissa has been chosen appropriately and all MTFs have been projected back into object space (i.e., the plane of the terrain model) using a magnification that reflects the 3.35-meter object distance and the maximum focal length used (about 120 mm). All of the component MTFs shown (for camera, lens, and low-pass filter) are estimates. In the lens case, the estimate is not the worst case because it does not affect the maximum radial off-axis position.

The estimated system performance shown is the product of the other three MTFs. Also shown is a curve representing an appropriately scaled high-contrast 22-centimeter target as seen by a possible flight camera from a distance of 50 meters.

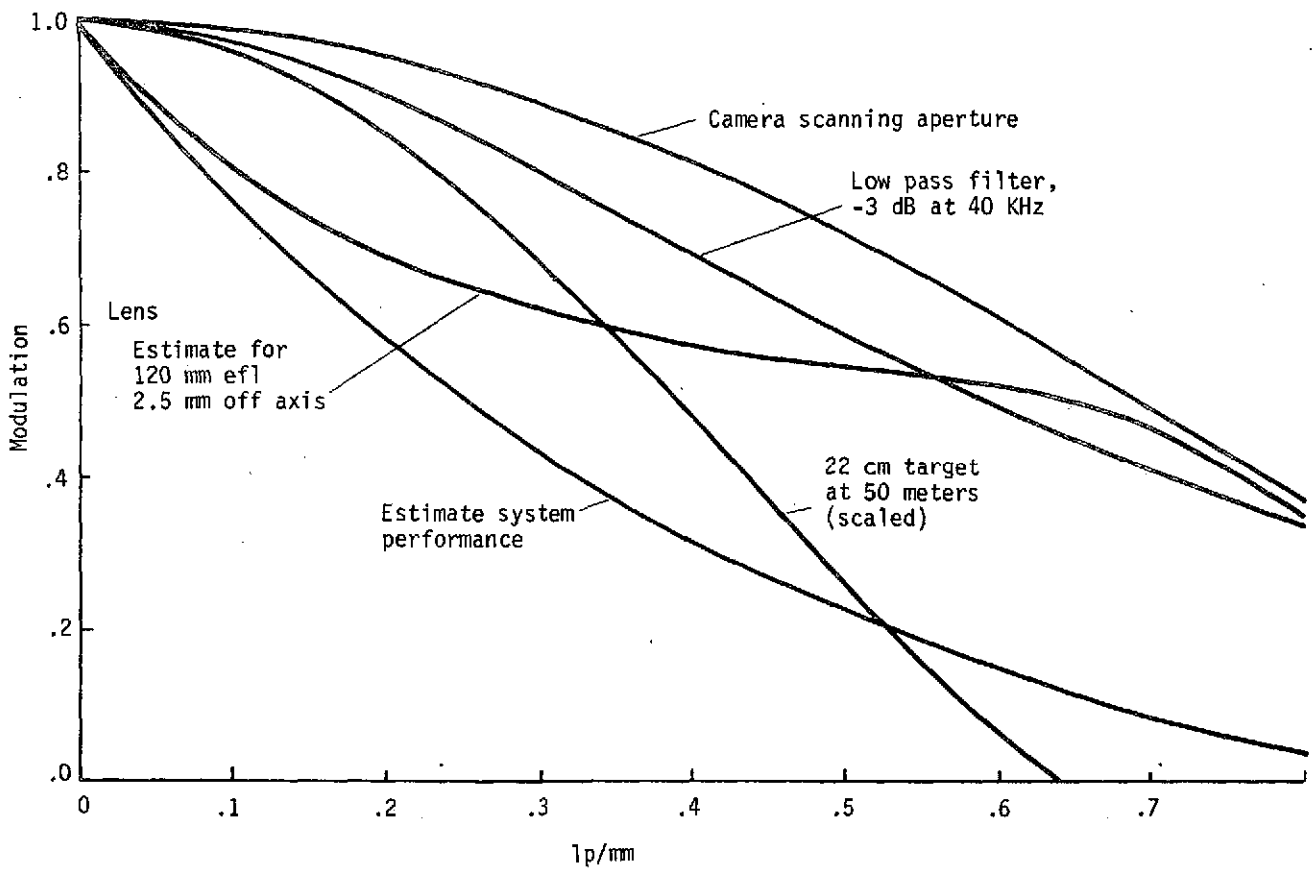


Figure 14.- Spatial Frequency In Object Space

MTF Measurement. - The goal of measuring the MTF of the video system was to place realistic bounds on performance expectations. It is also the best way to objectively evaluate how well the system has been assembled and adjusted. But most important in any feasibility demonstration of logic and signal processing is that the logic not be blamed for the failings of the camera system. Once information is filtered out of the video signal, it is lost forever and cannot be restored by any logic. This idea was considered particularly important since it was felt *a priori* that the laboratory camera is inferior to a flight camera.

The MTF was measured using the equipment illustrated in figure 15. The heart of the instrumentation was a PAR Model 160 boxcar integrator. This is essentially a sample-and-hold analog voltmeter whose sampling gate can be scanned with respect to a reference timing pulse. It is used to recover repetitive waveforms; in the present case, one scan line of video data. The auxiliary oscilloscope was used to provide improved time delay stability over that obtainable within the boxcar alone. Use of the boxcar integrator also improved the S/N ratio of the video signal through the averaging of many samples. The amplified and smoothed video signal was then fed to the Y input of an X-Y plotter. The X input was driven by a voltage level proportional to the time delay within a video line. The result is a plot of the video signal for one video scan line. Using high-contrast bar targets of varying spatial frequency, the modulation of the video signal could be calculated directly from the X-Y plotter record. The MTFs so derived are somewhat pessimistic at lower frequencies since they are square-bar MTFs and not the sine wave MTFs used theoretically.

Figure 16 shows MTF derived at the minimum camera altitude in the laboratory (for both maximum and minimum zoom focal lengths), for zero offset (the center subframe), and for an offset to a corner subframe. Also shown is a curve for a 22-centimeter high-contrast target scaled at 300/1. From these curves it is apparent that the MTF does vary with the subframe.

Figure 17 shows the same type of data at the maximum possible laboratory altitude. The effect of offset is shown to be less. The camera presented here for the 22-centimeter target is different because of its reference to flight conditions.

The effects of offset on the variation of MTF as a function of position on the photocathode are shown fully in figure 18. Here, MTF data derived at the maximum laboratory altitude for five positions along one diagonal are shown. Variations within a subframe were determined by controlling the time delay.

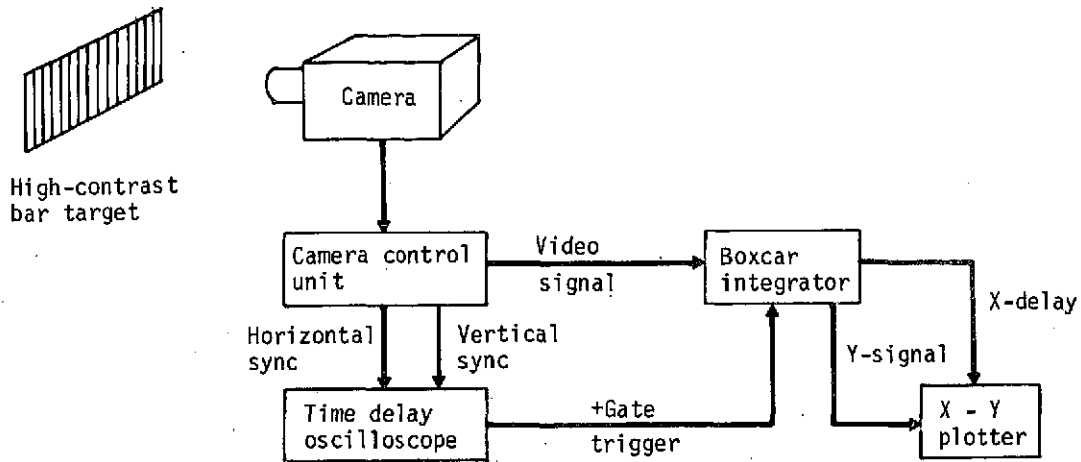


Figure 15.- MTF Measurement Scheme

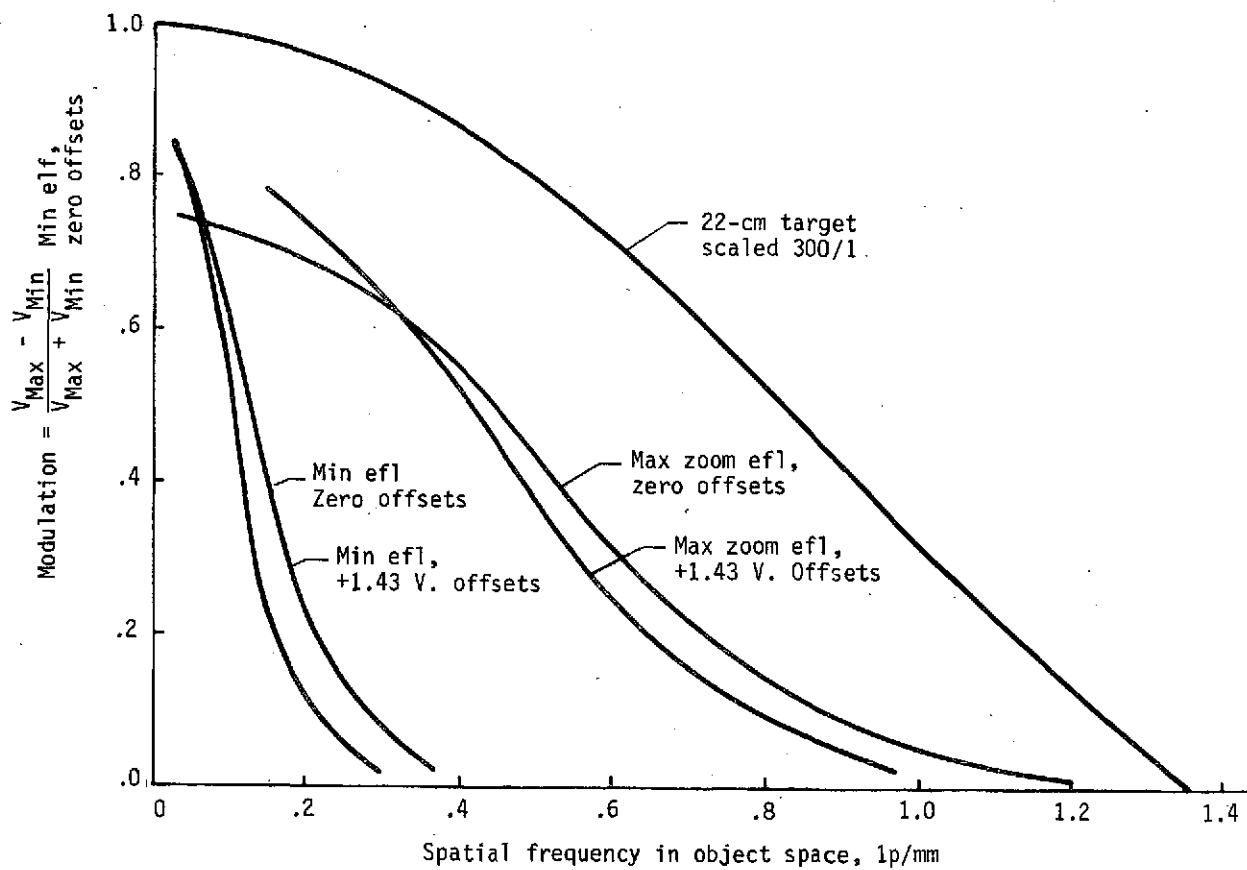


Figure 16.- Camera Modulation Transfer Functions, Minimum Laboratory Altitude

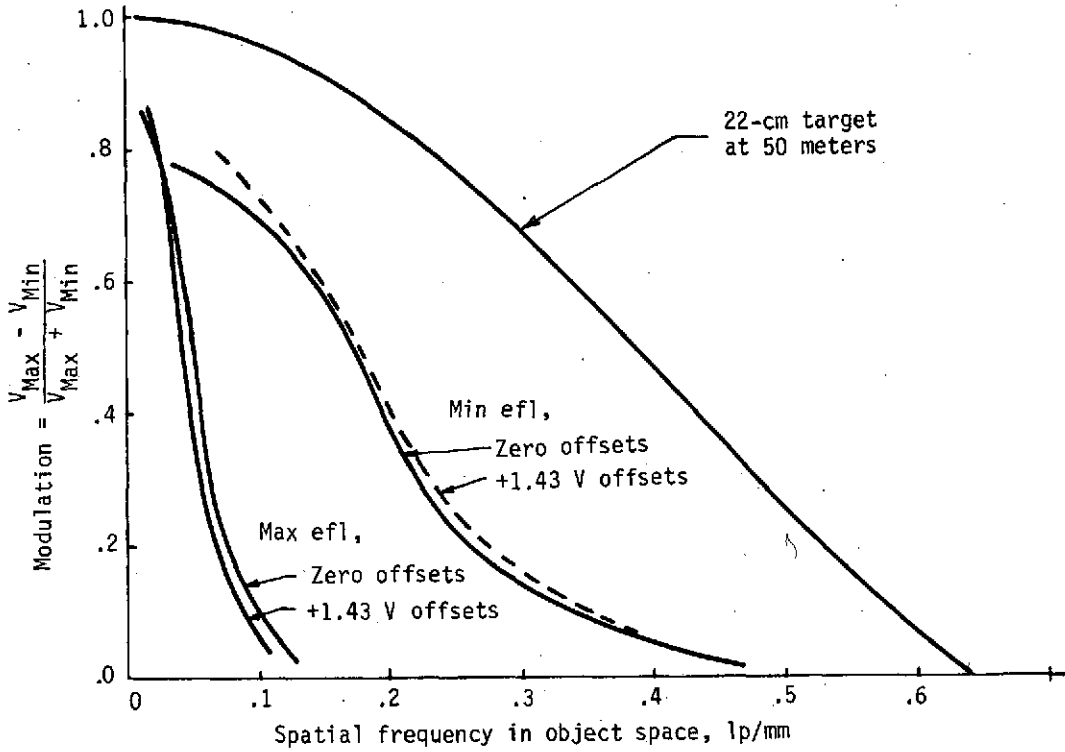


Figure 17.- Camera Modulation Transfer Functions

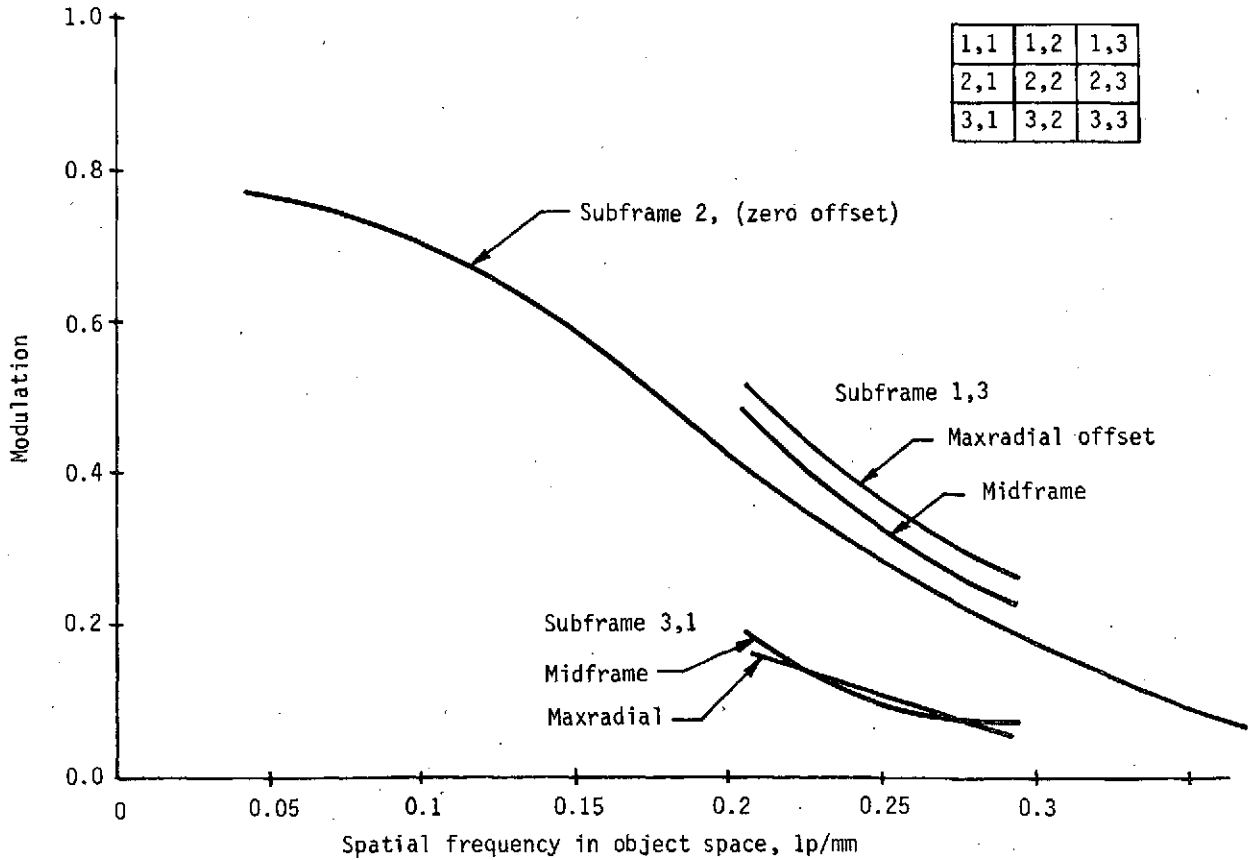


Figure 18.- Variation of Camera MTF between Subframes

The MTF measured for the laboratory system is, of course, not as high as would be expected in a flight system due primarily to the use of a zoom lens in the laboratory system. A flight system would use a high-quality fixed-focus optical system. However, use of the zoom lens to allow laboratory simulation of a large range of altitudes has in no way limited the usefulness and validity of the results obtained. The sizes of details in the laboratory were larger than the limiting resolution of the VGLIS system.

Algorithm Evaluation Experiments

The basic technique of comparing the ac portions of the video signal in various parts of the spectrum with the dc portion of the signal allows for an infinite variety of algorithms for rating each scene with a "figure of merit" for landing site suitability. Several questions must be answered before the technique can be reduced to hardware. The questions are as follows:

- 1) How should the signal components be compared?
- 2) Into how many bands should the spectrum of the video signal be divided?
- 3) How should the spectral components of the signal be measured--peak-to-peak, rms, absolute average, or some other way?
- 4) How should the comparisons at different parts of the spectrum be combined to get one figure of merit--linearly or nonlinearly? And if the combination should be nonlinear, how should it be done?
- 5) What weighting factors should be attached to the various spectral components? Should the weighting factors be a function of altitude?
- 6) Does an "optimum" system for distinguishing good areas from bad offer any significant advantage over a significantly simpler system? At what point do further improvements cease to be cost-effective in terms of mission success probability?

Although it was not possible to give definitive answers to all these questions, each was addressed in designing the breadboard system. As will be shown later, the experimental results

suggest that good results can be obtained even when these questions are answered in terms of practicality, cost, flexibility, and impact on existing spacecraft and laboratory hardware.

The first approach considered for comparison of the signal components was a time-domain technique in which each ac component was monitored to determine the amount of time the voltage was above a threshold compared to the amount of time it was below the threshold. Under near-ideal lighting conditions the approach worked well with fairly simple hardware, but when realistic lighting was used on a three-dimensional model, the ratings did not correlate well with site desirability. When methods for reducing sensitivity to lighting were considered, the required hardware became so complex the approach was abandoned in favor of a different method.

When a linearly responding photocathode is used in the camera, the ratio of ac component in the video signal to dc component is approximately constant for a given scene regardless of the illumination intensity over a light intensity range of more than 4 to 1. If the ac voltages and the dc voltage could be measured, the ratio would be an index of surface roughness. This is the approach used in the experiments.

Experiments with test targets were conducted to determine what frequency ranges best distinguished high-contrast targets from low-contrast targets. Although these tests did not show any great advantage in dividing the ac component into bands to determine surface ruggedness, certain rough areas were best distinguished from others in the bands from 30 Hz through 9 kHz and from 1 through 30 kHz. These bands were used in the experiments to allow flexibility--weighting factors could be changed with altitude, for example, or different parts of the spectrum could be emphasized without hardware change. But the exact cutoff frequencies that distinguish among targets best are nebulously defined even for specific targets, and, as will be mentioned later, the experiments suggest that for a flight version of the system there is no clear advantage in breaking up the ac component of the video signal into bands. The feasibility experiments were conducted with the two band filters acting essentially as one.

The ac components of the signal were measured with circuits that respond to average absolute value rather than a rms or peak-to-peak value. This was done because the circuits were simpler to implement and because the other techniques offered no clear advantage.

Before the filter outputs could be combined to form a figure of merit, a method had to be found to correct for noise and offset voltages in the three analog signals so the ac-to-dc ratios would be constant for a given scene regardless of light level. When the ac outputs for a scene are plotted as a function of the dc output as light intensity is changed, the graphs are straight lines whose slopes are characteristic of the scene. The offset voltages are found from the graphs at the point where the lines for different scenes intersect. Instead of a simple ratio of ac component to dc component then, we have

$$V_{ac} \text{ (Normalized)} = \frac{V_{ac} - V_{\text{Offset 1}}}{V_{dc} - V_{\text{Offset 2}}}$$

In sunlight the corrections would be less significant, but in the laboratory situation where relatively weak lighting was used, the corrections significantly reduced the system's sensitivity to lighting.

Two experimenters rated 14 scenes subjectively for site suitability and plotted their ratings on a graph of normalized midband output versus normalized high-band output for the scenes. For scenes from the surface model, the two normalized outputs were small for scenes with good ratings and large for scenes with bad ratings. However, the two outputs were so nearly proportional that each alone was a good index of site suitability, and no nonlinear method of combining them to form one rating appeared to offer any advantage over a linear combination. The figure of merit used then, was simply

$$\text{Rating} = a \left(\frac{|\bar{V}_M| - b}{|\bar{V}_L| - c} \right) + \left(\frac{|\bar{V}_H| - d}{|\bar{V}_L| - e} \right)$$

where $|\bar{V}_M|$, $|\bar{V}_H|$, and $|\bar{V}_L|$ are the midband, high band, and dc components' average absolute values, respectively. Although a single filter could be substituted for the two ac filters with essentially the same results, the flexibility of having two filters in the breadboard version of the system was useful because it allows future experiments with altitude-dependent ratings.

The sequence of pictures shown in figure 19 was taken from the console television monitor during an experiment using the algorithm described previously. In actual operation the nine areas are scanned sequentially. They are shown here simultaneously for improved visual presentation. After the nine areas are scanned the center of the area with the least amount of contrast is selected as the desired landing site. The scan is then repositioned by moving it toward the desired landing site while keeping the new field of view within the old field of view. The final site (the center of the last photograph) is the result of 20 observations and decisions.

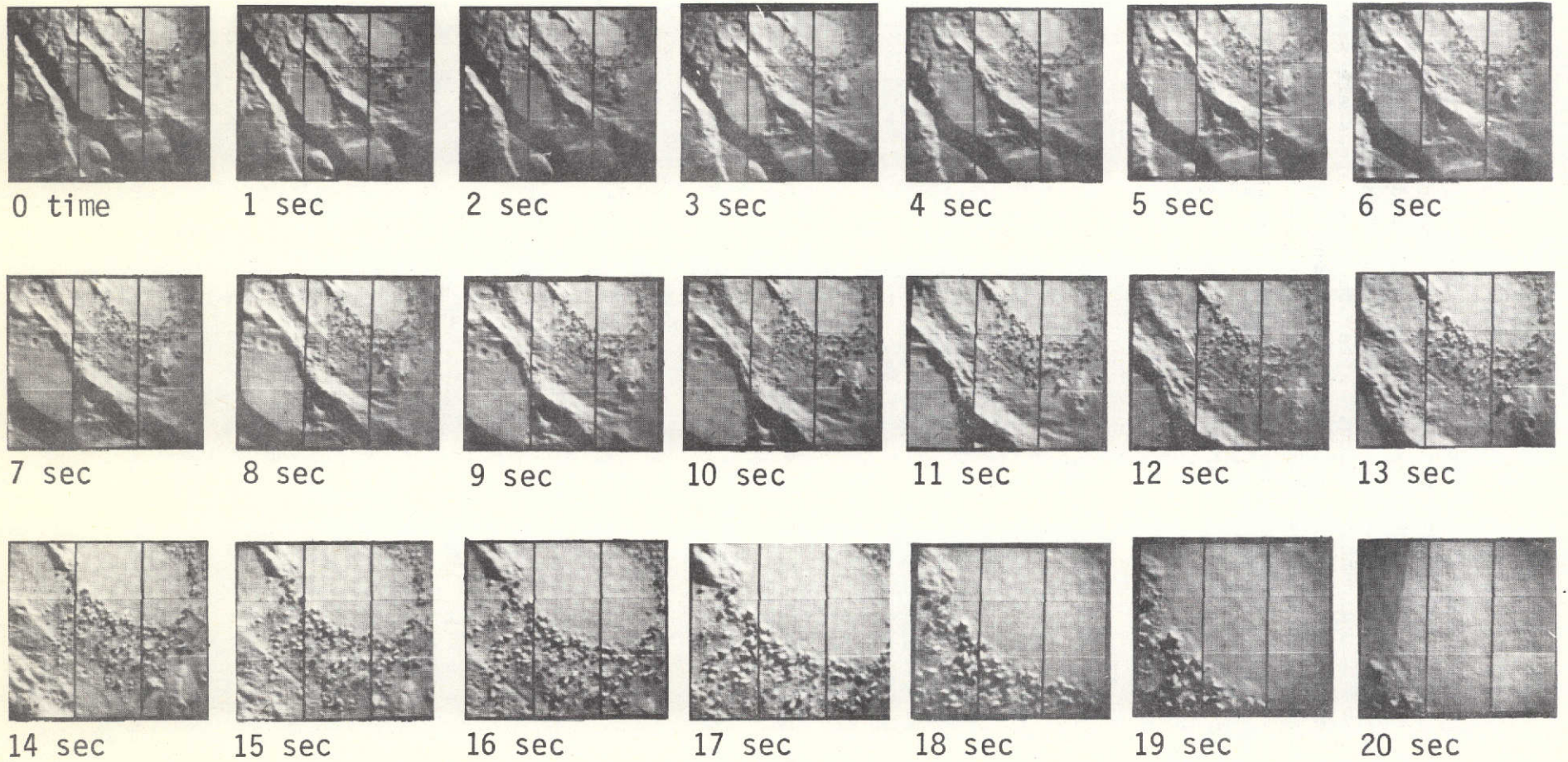


Figure 19.- Monitor Observations for a Typical Experiment

Monte Carlo Experiment

The system computer was programmed to select an initial simulated altitude between 500 and 900 meters and an initial position above the three-dimensional Martian surface model at random using a random number generator. It then calculated altitudes and predicted impact points for the lander as it approached the surface under system guidance. The computer received guidance information 20 times during the descent. When the simulated altitude reached 100 meters, the predicted impact point was recorded on tape but not printed so the experimenters who were to rate the selected sites would not be biased by seeing the sites picked. After each landing, the computer selected a new set of random initial conditions and repeated the procedure without operator intervention until 50 landings had been simulated.

Two experimenters who did not observe the Monte Carlo run each ran a second program to rate the sites. Because the ratings were of necessity somewhat subjective, it was desirable to see if the results would depend greatly on the individual doing the rating. The experimenters therefore worked alone in rating the sites.

The computer read the tape and positioned the camera to display each selected site on the system monitor. It also selected a large number of sites entirely at random and presented selected and random sites in random sequence. The experimenters therefore never knew whether the scene they were rating was one selected at random or one from the tape. This was done to eliminate experimenter bias for or against system-selected sites.

For each scene, the experimenter observed the corresponding spot on the model and gave his estimate of the probability that a landing there would be successful. This estimate assumed that the lander was functioning normally and did not consider failure modes unrelated to the landing site. The computer used the random number generator to determine from this rating whether the landing was a success or failure. (For example, if the experimenter gave a 50% survival probability, the computer picked a random number after assigning half of all possible numbers as successes and the other half as failures.) The computer printed the success/failure record for each scene.

The results obtained by the two experimenters agree closely and show the system to be very effective. Without guidance only nine out of 48 landings (19%) were successful according to the first experimenter's ratings, and six out of 40 (15%) were successful according to the second experimenter's ratings. These

numbers are for the randomly selected sites, which were different for each experimenter. Using the optical guidance system, 44 out of 50 (88%) were successful according to the first experimenter's ratings, and 42 out of 50 (84%) were successful according to the second experimenter's ratings. Although the system did not always choose the best possible site, it successfully avoided sites the experimenters rated as having a success probability of less than 75%. In contrast, the unguided landings were frequently in locations where success probability was essentially zero.

The conditions modeled in the experiment were as tabulated.

Sun angle -- approximately 60 deg from normal to the surface.
View obstructions (clouds, dust storms, etc) -- None
Surface features -- Typical of scientifically interesting area, including both hazardous and smooth areas visible for each initial condition.
Color -- shades of gray.
Guidance mode -- Constrained not to leave camera field of view.
Number of subframes per decision -- 9 in a 3x3 matrix
Number of guidance decisions -- 20
Spacing of decisions -- Uniform with altitude.

The fact that initial conditions were randomly selected allows one to draw the following conclusions about landing in the modeled area as a whole with the guidance mode given in table I.

TABLE I.- VGLIS SUCCESS PROBABILITY

	Using experimenter 1 ratings	Using experimenter 2 ratings
50% confidence limits for proportion of success with guidance	85% to 91%	80% to 84%
90% confidence limits for proportion of success with guidance	77% to 94%	72% to 92%
50% confidence limits for proportion of success with- out guidance	15% to 23%	12% to 19%
90% confidence limits for proportion of success with- out guidance	10% to 32%	7% to 28%
Minimum improvement in pro- portion of success based on 50% confidence limits	62 percentage points	61 percentage points
Minimum improvement in pro- portion of success based	45 percentage points	44 percentage points

MISSION CONSIDERATIONS

Lander Constraints and Propulsion System

The Viking terminal descent system must accomplish navigation, guidance, and control functions to successfully land the capsule on the Martian surface with prescribed vehicle velocity and attitude. The velocities required at landing are:

- 1) Horizontal velocity - 0 ± 1.22 m/s (0 ± 4 fps);
- 2) Vertical velocity - 2.44 ± 0.91 m/s (8 ± 3 fps).

The lander roll axis must be oriented within 5 degrees of local vertical at landing and an rss attitude rate of 0 ± 7 deg/s in pitch and yaw is required. To maintain radar lock, attitude rates of greater than 30 deg/s [rss (pitch, yaw)] are not permitted during terminal descent.

To accomplish a soft landing, the three components of the lander's velocity measured with respect to the surface must be controlled as a function of altitude measured with respect to the surface. Because lander system studies have shown that multiple, differentially throttled monopropellant engines are the most efficient retroengines, they were selected for propulsion during the descent. Following is a summary of Viking descent guidance laws.*

Gravity-turn steering was selected as the means of controlling the lateral velocity components. This law is mechanized by rotating the vehicle about its pitch and yaw axes until the lateral body-axis velocities are zero. This causes the thrust axis to point along the total velocity vector. This steering law is simple to mechanize because local vertical sensing is not required. Gravity causes the thrust axis to rotate toward the vertical as the velocity is reduced. An arbitrary roll orientation is maintained by using an attitude-hold mode during the descent. If the components of vehicle velocity are denoted as u , v , and w along the roll, pitch, and yaw axes, respectively, then the steering signals are

$$\text{Pitch: } \alpha_c = G_\alpha w/u$$

$$\text{Yaw: } \beta_c = G_\beta v/u$$

$$\text{Roll: } \phi_c = 0$$

* R. F. Broderick, *et al.*: *Terminal Descent Simulation Study*. NASA CR-66811. Martin Marietta Aerospace, Denver, Colorado.

where G_α and G_β are the pitch and yaw gains, respectively. These signals generate attitude commands that drive lateral velocities to zero.

The axial component of velocity, u , is controlled by modulating the vehicle thrust to follow the preprogrammed desired velocity/altitude contour shown in figure 20. The navigator estimate of altitude is used to calculate a desired velocity from the contour. This desired velocity (V_D) is then compared with the navigator estimate of velocity (V) and a throttle setting is computed that will cause the vehicle to follow the contour, that is;

$$t = G (V - V_D) + b$$

where t is throttle setting, G is the control system gain and b is the throttle setting about which modulation occurs. The control system gain varies as a function of remaining fuel. The contour is designed for all velocity conditions resulting from winds during the parachute phase, and is shaped to account for propellant tank pressure blowdown and specific impulse changes. After a 2-second engine warmup, the parachute is jettisoned and a 3-second maneuver phase is allotted for aligning the thrust and velocity vectors. A high thrust phase is designed to command up to 84% of the available thrust, this will conserve propellant by minimizing gravity losses. The remaining thrust is used for steering and to provide thrust margin. A constant-velocity phase allows the vehicle control system to reduce the effects of dynamic control lags and errors that result from following the high-thrust phase contour before shutting down the engines.

The lander, depending on initial velocity, follows the maximum or minimum contour or, if the initial velocity is between the maximum and minimum, the lander will fly a contour that is a constant percentage of the distance between the minimum and maximum contour.

Simulations have shown that this approach allows margin for any 30 combination of atmospheres, winds, and surface slopes. The minimum velocity resulting from the parachute phase occurs in the maximum-density atmosphere with zero wind. The resulting trajectory has a long drop phase before intersecting the design descent contour for the high-thrust phase. The propellant required for this condition is less than that required for the maximum wind case.

The propulsion system design parameters of blowdown ratio, maximum thrust, throttle ratio, and propellant loading are defined through descent simulations using the guidance laws described above. The thrust and blowdown ratio was chosen to minimize the weight of the system.

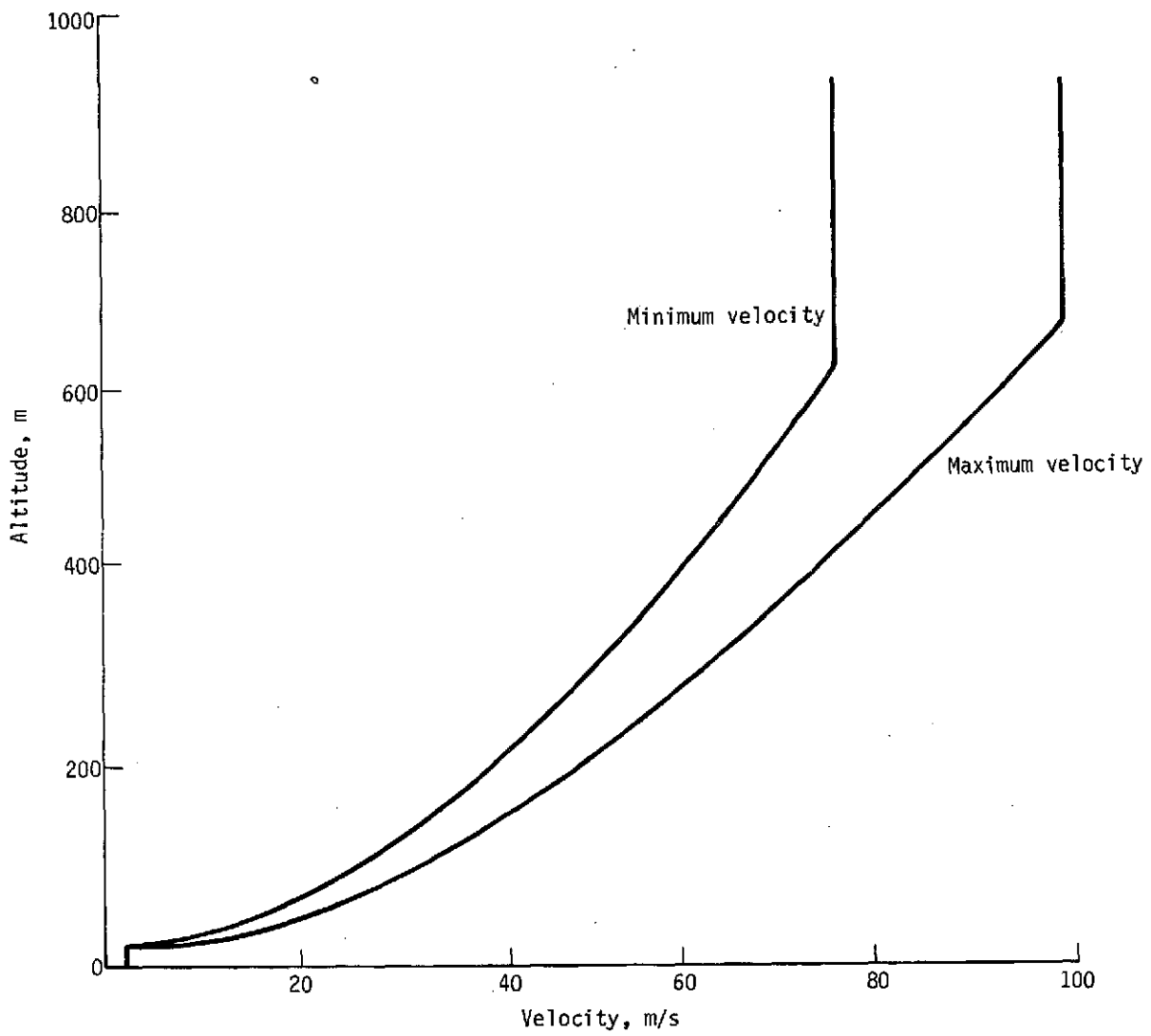


Figure 20.- Viking Velocity - Altitude Descent Contour

Impact of Additional Fuel on Propulsion System

The Viking propulsion system and guidance and control laws are the result of careful analysis and provide adequate performance with a minimum weight penalty. Adding an additional 10 kilograms of fuel to the current fuel tanks would require the removal of pressurant to keep the tank pressure at a level below the limits of the valves. If valves that could take higher pressure were used, more thrust would be available but the propulsion system would blow down differently. Viking personnel indicate that valve redesign is not practical. The diameter of the two fuel tanks can be increased from 0.6 to 0.63 meter. This allows the addition of 10 kg of fuel to the current 60.1 kg of fuel and the addition of a corresponding amount of pressurant to provide identical thrust, tank pressure, and blowdown characteristics. With this implementation of the additional 10 kg of fuel, the lander can hold high-thrust levels for a longer period of time but cannot provide instantaneous thrust higher than that of Viking '75.

Maneuver Capability

A guidance scheme ultimately must be designed for site selection maneuvering. This guidance scheme will depend both on propulsion characteristics and on the site selection sensor characteristics. Because a firm sensor system design does not exist, the maneuver capability estimation was performed based on propulsion characteristics with no regard for the sensor's effect on maneuver capability. However, a discussion of maneuver capability considering sensor characteristics is presented later in this report.

Two approaches were taken for maneuver capability analysis:

- 1) Estimate maneuver capability by performing tip-up and then perturb the gravity turn guidance logic for down-range and crossrange excursions;
- 2) Estimate maneuver capability by performing a gross maneuver, performing tip-up and following the gravity turn guidance logic to the ground.

In practice a combination of the two approaches would provide considerable maneuver capability.

The following conditions existed for both approaches:

- 1) Lander weight = 645 kg;
- 2) Propulsion characteristics as described previously;
- 3) Site selection sensor constraints were ignored;
- 4) Initial altitude = 863.5 m;
- 5) Total velocity = 97.8 m/s;
- 6) Flight path angle = -50.11 deg;
- 7) Initial vehicle attitude has inertial pitch of 0 and yaw of 0, i.e., thrust vector pointed straight up. Roll was ignored;
- 8) Horizontal velocity vector is in same direction as planet rotation;
- 9) Vehicle is directly over the equator.

The initial conditions represent the maximum velocity conditions resulting from winds during the parachute phase. These conditions were used because they require maximum fuel consumption. The trajectory is plotted in figure 21.

Analysis for maneuvering by making small deviations from the gravity turn was performed using the MOD6MV computer program. MOD6MV is a modularized six-degree-of-freedom trajectory program with the capability to simulate orbiting vehicles and planetary landers of various types and is documented under NASA Contract NAS1-8913. The MOD6MV can simulate all phases of the Viking mission; however, only the terminal descent phase has been modified to include the capability of the video guidance system. Figure 22 depicts the guidance and control system for the powered portion of the terminal descent phase including the functions of the video guidance system. The MOD6MV program provided the basis for the vehicle control and dynamics. The digital simulation models that functionally describe sensor operation and the additional flight computer software for the video guidance system have been added, along with a surface model designed with the capability to generate and display a digital grey level representation of various surface features.

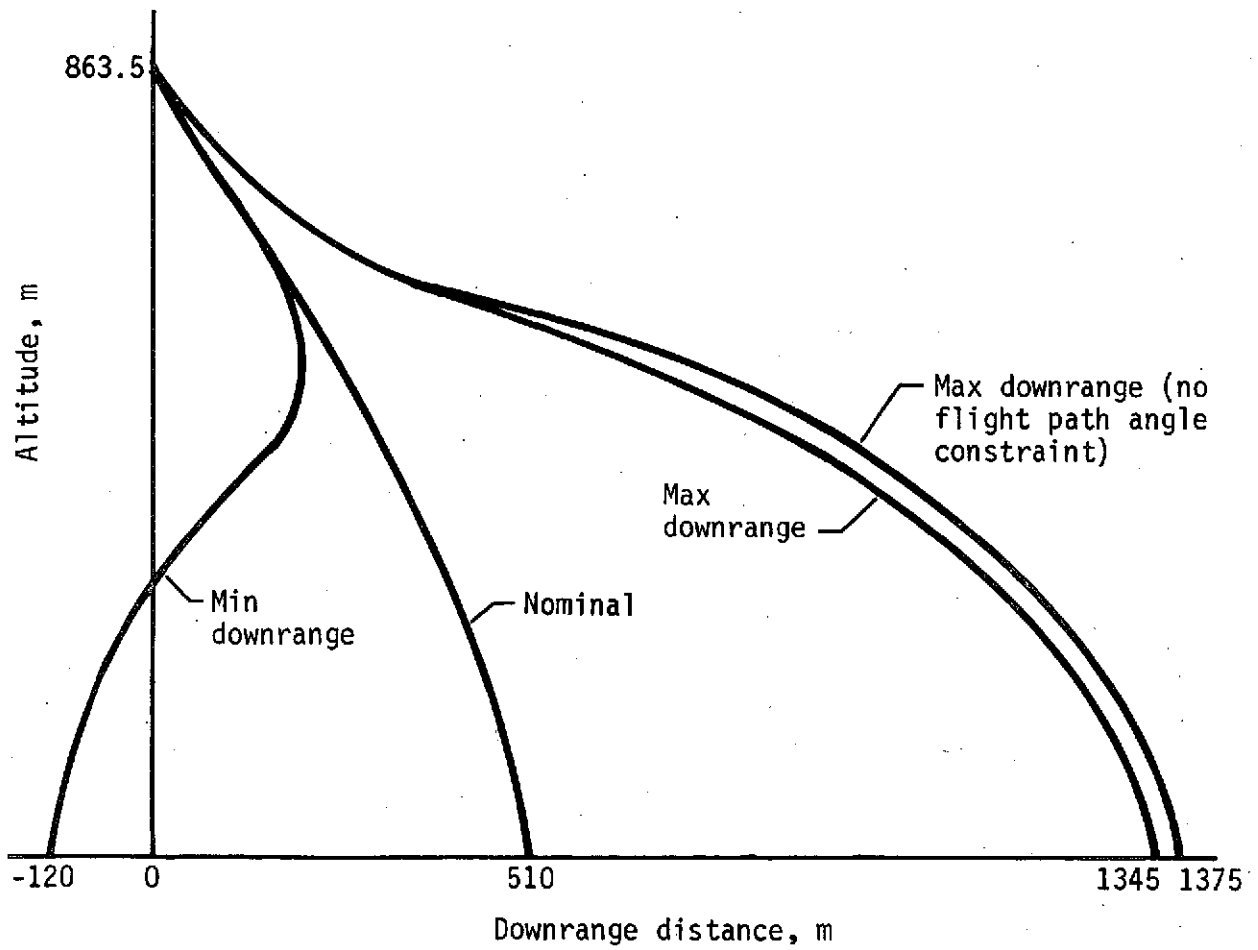


Figure 21.- Viking Maximum Maneuver Capability

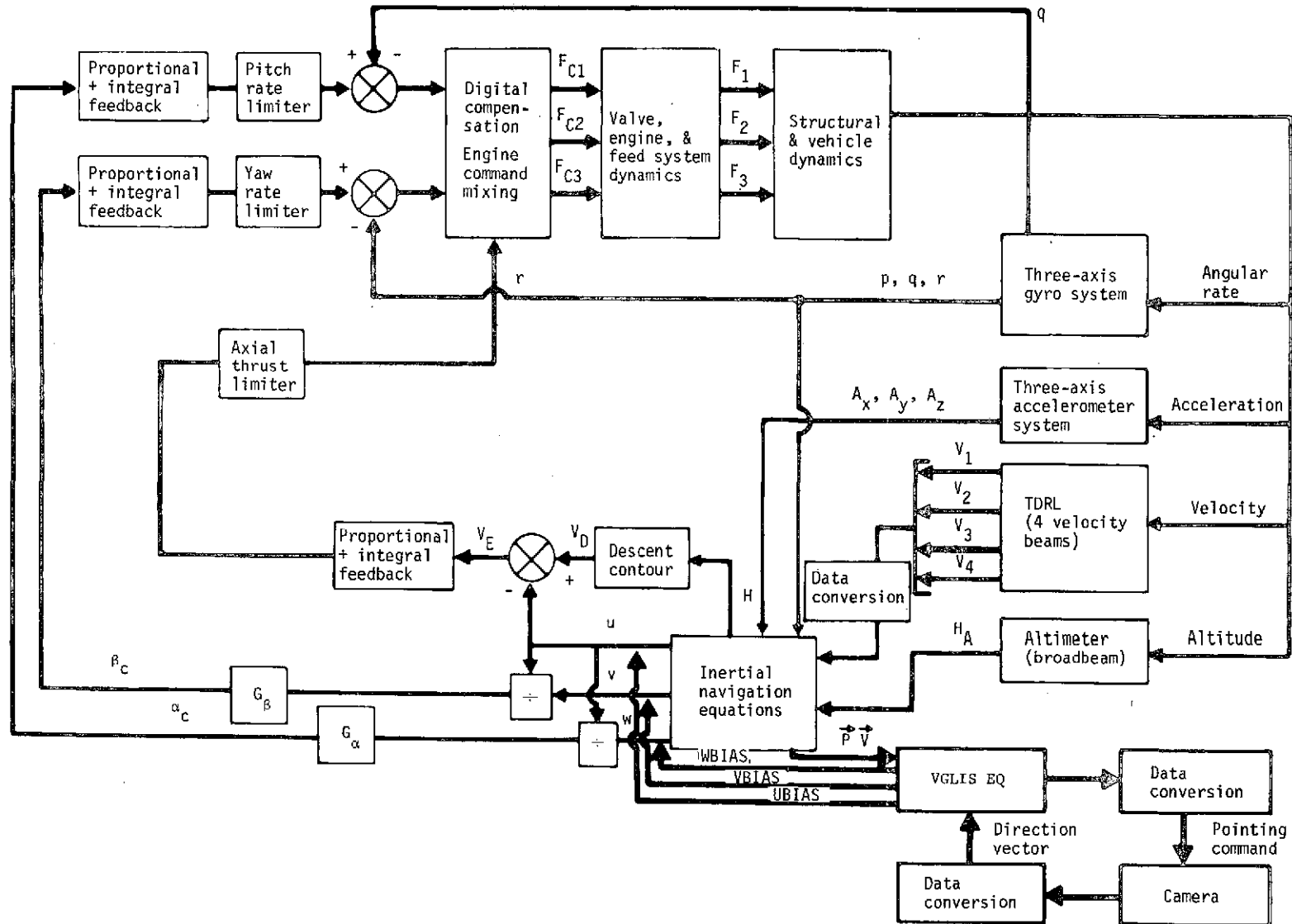


Figure 22.- Terminal Descent Guidance and Control System

The throttling and propulsion portion of the program was used to determine the maximum maneuver distance possible while satisfying constraints at landing. This was done by determining the magnitude and direction of a bias velocity vector (as a function of time) that caused the lander to land at a particular point. Runs were then made to move that point away from the nominal landing point until the lander crashed. Using this technique, the small landing footprint illustrated in figure 23 was obtained. This is a rather small area but little additional fuel is required, about 1.59 kg (3.5 lb). The lander follows the altitude-velocity contour except that the thrust vector is oriented to reach the desired point and not oriented opposite the velocity vector. A crash occurs when the angle between the velocity vector and the thrust vector becomes so large the control law cannot remove the velocity error. The control law gain was chosen assuming that thrust is opposite velocity. It appears to also have the capability to remove velocity error when thrust is oriented within a limited region about the velocity vector, thus allowing some maneuver capability. When using a video guidance system, a control law should be designed that corresponds to the specific guidance system characteristics such as field of view and scan positioning logic as well as propulsion characteristics.

The additional 10 kg of fuel cannot be used without a significant departure from the Viking flight plan. Additional maneuver capability for the 10 kg of fuel was determined by performing a large pitch or yaw maneuver before going to a gravity turn. This maneuver would result from VGLIS site selection commands based on data collected during the parachute phase. The lander then held this attitude and throttled at maximum thrust for a specified amount of time. Next the lander performed the tip-up maneuver, aligning the thrust and velocity vectors, and followed the nominal altitude-velocity descent contour to the ground. The tip-up maneuver was performed at a high thrust level instead of the current low thrust level. The large landing envelope illustrated in figure 23 was determined in this manner. The magnitudes of the pitch or yaw maneuver and the burn time following the maneuver were determined using the POST (program to optimize simulated trajectories) program. POST is a digital three-degree-of-freedom simulation that provides the capability to optimize trajectories for launch, entry, and orbital vehicles in both atmospheric and exoatmospheric flight. The program was developed, documented, and validated under NASA Contract NAS1-10811. The generality of the program is evidenced by its N-phase capability, optimization by the discrete parameter technique, generalized targeting and stopping variables, static trim capability, oblate planet generalized atmosphere model, atmospheric winds, inequality constraints, and generalized table inputs. The general nature of this program allows modeling, by input, the Viking lander blowdown engines by a bivariate table of thrust values as a function of the remaining fuel and throttle setting.

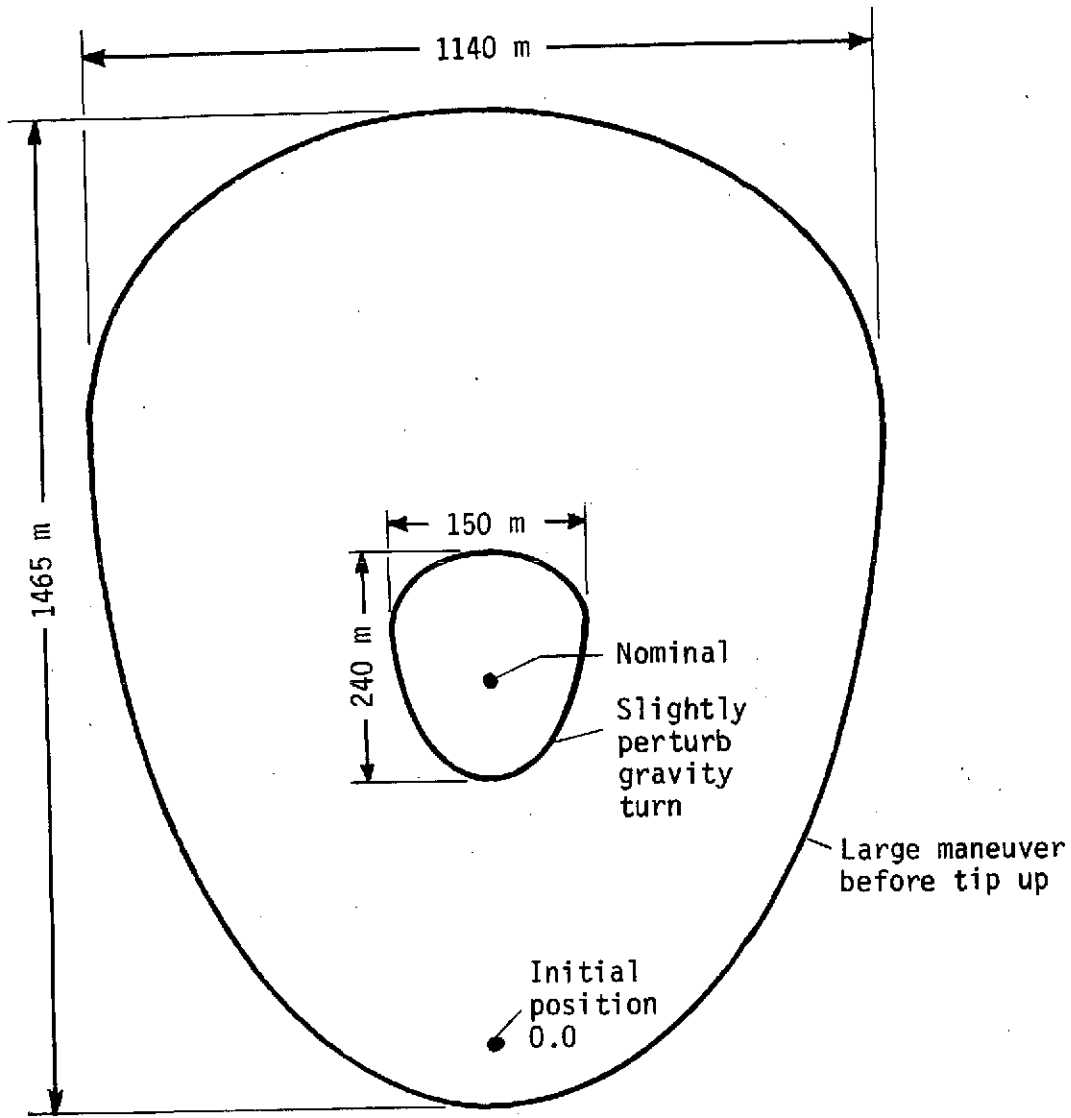


Figure 23.- Maximum Maneuver Capability - Footprints

The inequality constraints allow the final velocity and attitude requirements to be met before landing. A program module is provided for implementing steering and throttling laws. Program statements were added to the module for computing the accelerations required to follow the terminal descent contour after the maneuver.

A brief description of the program operation will be given to clarify the selection of maneuver parameters.

Suppose we wanted to find the point (X, Y) that lies within the circle $X^2 + Y^2 = 4$, for which X is a maximum (fig. 24). Clearly the answer is (2, 0), but suppose the problem cannot be solved by inspection. Using the optimization technique in POST one would make a guess at the answer and POST would attempt to find the actual solution. Suppose we made an initial guess of (-3, 3) as indicated in the figure. POST would first check to see if the guess satisfied the constraint that the point lies within the circle $X^2 + Y^2 = 4$. It does not, so POST chooses the closest point on the circle. Now that the constraint is satisfied, POST tries to maximize X. A new point is chosen in the direction of the gradient of X, i.e., the direction in which the magnitude of X increases most rapidly; however, this point must also satisfy the constraint. The point chosen has the same Y-coordinate but a larger X-coordinate. Next POST would take a series of steps around the circle as illustrated in the figure until the value of X is a maximum and the point (2, 0) is selected.

This optimization and targeting capability was used to determine the parameters to achieve maximum maneuver capability.

Consider the case of maximizing the downrange maneuver distance. A profile to increase downrange distance from that obtained from following the nominal trajectory would consist of a pitch maneuver to an attitude that would permit the vehicle thrust to decrease the descent velocity and increase the horizontal velocity in the downrange direction. After this attitude is reached, full thrust is applied for a specified time. Then the tip-up maneuver is performed, that is, another pitch maneuver is performed to thrust opposite the velocity vector and the terminal descent contour is followed to the ground.

POST was used to determine the magnitude of the pitch angle and the duration of the burn that will give maximum downrange travel subject to constraints on final velocity and attitude. The initial investigation revealed that the portion of the Viking control law programmed in POST had no difficulty in eliminating velocity errors after the maneuver and following the altitude-velocity

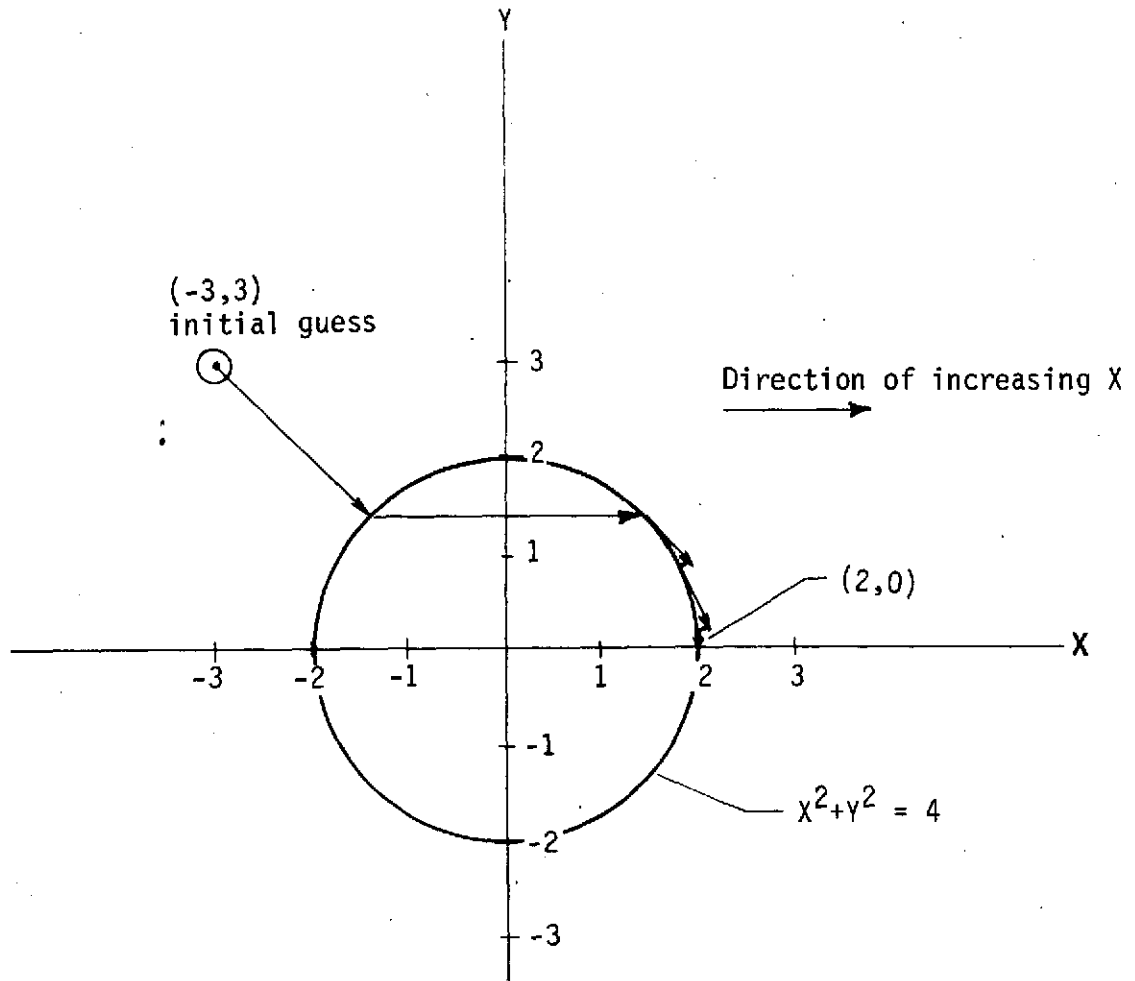


Figure 24.- POST Optimization Algorithm

contour to the ground. Thus all landing velocity and attitude requirements were met. It also became apparent that it was not necessary to simulate the trajectory all the way to the ground.

Because no maneuvering is allowed during the constant-velocity phase, all digital simulations were terminated at an altitude of 13.72 meters (45 ft). This is valid provided there is adequate fuel remaining to complete the descent. Fuel consumption during the constant-velocity phase is approximately 0.46 kg/m (0.3 lb/ft). This requires fuel remaining of 6.12 kg (13.5 lb). On the advice of Viking project personnel, this was increased to 6.8 kg (15 lb) to allow some margin. The problem solved by POST then became: Determine the magnitude of the pitch maneuver and the duration of the burn that will yield maximum downrange distance subject to the constraint that there be at least 6.8 kg (15 lb) of fuel remaining at an altitude of 13.72 meters (45 ft). The solution to this problem was

Pitch angle = -21.83 deg

Burn time = 3.59 s

Downrange = 1376.8 m (4517 ft)

Remaining fuel = 6.8 kg (15 lb).

The resultant trajectory is plotted in figure 21. During this flight the vehicle flight path angle (measured from local horizontal to velocity vector) came to -11 degrees. This could cause radar lock to be lost (the limit is -15 deg). Viking project personnel indicated that loss of lock for less than 10 seconds would not cause any problems. However, to be somewhat conservative in the maneuver distance estimates, this constraint was considered. Table II presents the history of values obtained by POST to solve this problem. Table III summarizes the final values for maximum and minimum downrange (figure 21), and maximum crossrange (figure 25).

These numbers represent estimates of maneuver distances that can be obtained by expending all available fuel in an optimum manner for the initial conditions previously described. Additional maneuver capability can be obtained with the same fuel allotment by beginning to maneuver at a higher altitude. The lander velocity vector is relatively constant during the last 300 meters of the parachute phase and the site selection process could start at any time by jettisoning the parachute earlier.

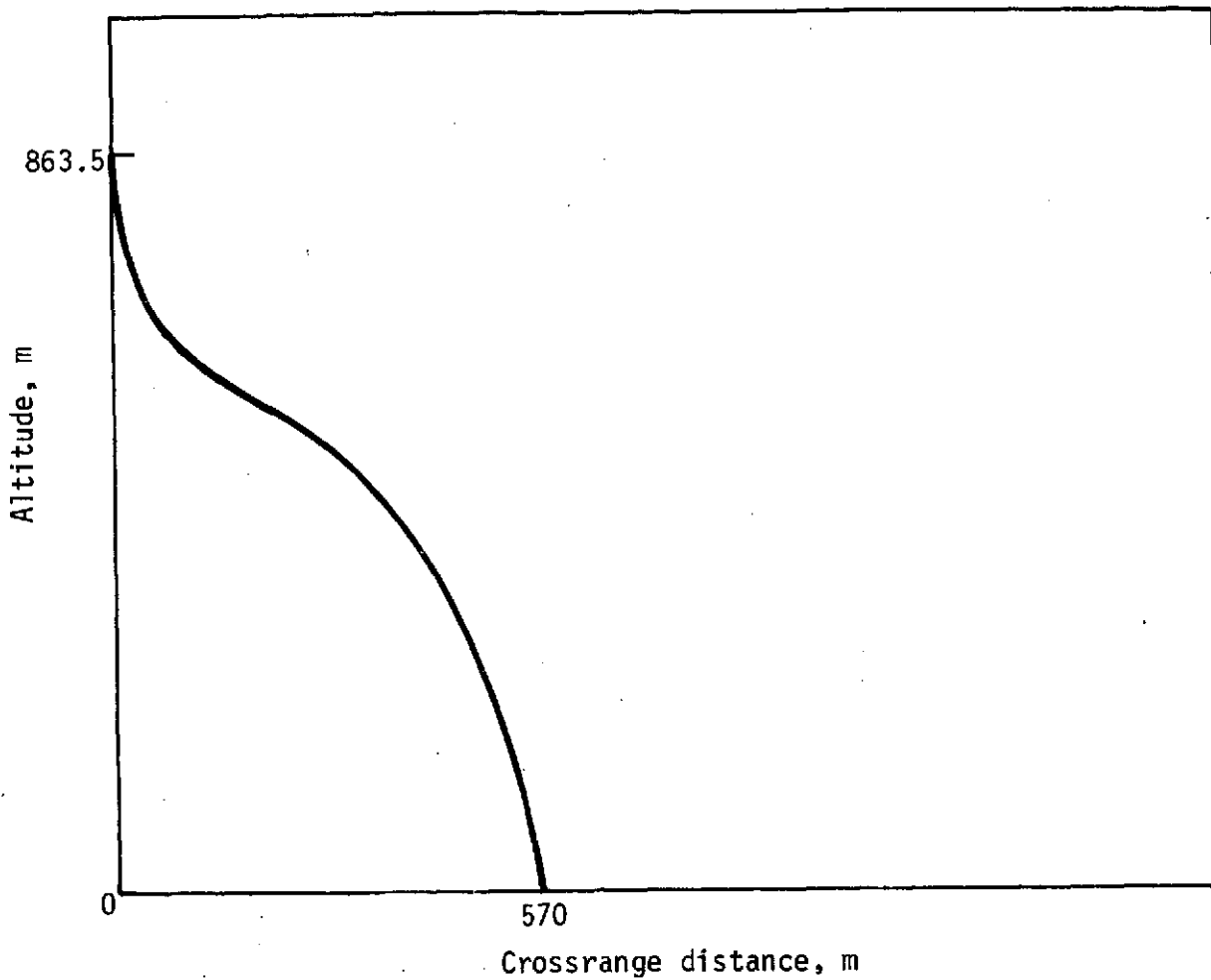


Figure 25.- Crossrange Maneuver Capability

TABLE II.- POST ITERATION HISTORY

Iteration number	Pitch deg	Burn time, s	Remaining fuel, kg	Maximum flight path angle, deg	Down-range Dist, m	Comments
0	-60.0	1.5	2.13	-17.73	1370	This is initial guess; note fuel error.
1	-59.9	1.49	2.29	-17.8	1360	Fuel is improving.
2	-48.8	1.42	6.85	-19.4	1245	Both constraints are satisfied. Note loss in downrange.
3	-41.2	1.96	6.95	-17.7	1290	Both constraints still satisfied. Downrange improved.
4	-32.4	2.68	6.79	-15.0	1345	Solution--fuel and flight path angle are at limits.

TABLE III.- MAXIMUM MANEUVER DISTANCES

	Attitude maneuver, deg	Burn time, s	Maneuver distance, m
Maximum downrange	Pitch - 32.4	2.68	1345
Minimum downrange	Pitch + 55.6	7.11	-120
Maximum crossrange	Yaw + 31.8	3.83	570

Considerations for designing a control law for a video guidance landing and imaging system must evaluate the characteristics of the site selection sensor and the associated gimbal authority and scan positioning logic. A vehicle such as Viking must perform an attitude maneuver in order to perform a crossrange or large downrange maneuvers. The new vehicle attitude may make it impossible to see the point to which it is flying depending on sensor gimbal authority. The effects of scan positioning logic are more subtle. For example, previous work* presented a sensor system with an instantaneous field of view of 12 degrees broken up into 9 areas.

*R. T. Schappell and G. R. Johnson: "Experimental and Simulation Study Results of a Planetary Landing Site Selection System." *Journal of Spacecraft and Rockets*, Vol 10, No. 4, April 1973, pp 277-280.

The impact point was predicted and the scan was centered about it. The center of one of the nine areas was chosen as a more desirable impact point and the necessary maneuvers were begun to reach that point at the time of impact. One second later a new impact point was predicted. This prediction assumed that the maneuvers already performed would be the only maneuvers performed. Thus, the new predicted impact point lies on a line between the original impact point and the impact point selected by the previous scan. This process continues until the lander reaches a minimum operating altitude. The site selection logic always chooses a point within its current field of view and the size of the field of view is always decreasing. The net effect of this process is illustrated in figure 26. This figure shows how the field of view decreases with altitude and how the predicted impact point moves. The upper right-hand corner was chosen as the desired landing site after every scan. This represents the maximum maneuver capability for this particular landing site selection system. Note that the propulsion system is not the only limiting factor. The fact that each successive scan was positioned close to the previous scan was the limiting factor. Nevertheless this landing site selection system was quite stable and effective.*

A landing on the simulated surface depicted in figure 27 was attempted using this landing site selection system. The series of pictures in figure 28 illustrates the visual aspects of this landing. Move from left to right and top to bottom, the field of view is seen to decrease in size and increase in detail as the lander descends and ground resolution improves. The arrows under each picture indicate the maneuver direction chosen based on surface characteristics. The last three pictures are not full size because the digital surface grid point spacing does not allow enough points to plot at the full size and maintain reasonable "picture" quality.

Maneuver capability can be increased by positioning the scan differently. For example, the scan could be centered about the preferred landing site (A, fig. 29). This could cause points to be chosen outside of the initial field of view and to ultimately choose a point that was out of maneuver range. This process would not make efficient use of fuel since additional downrange or cross-range could be requested as altitude decreases. In addition new surface features are being processed during descent. This makes it possible to land on a large feature that would have been avoided

*Ibid. R. T. Schappell

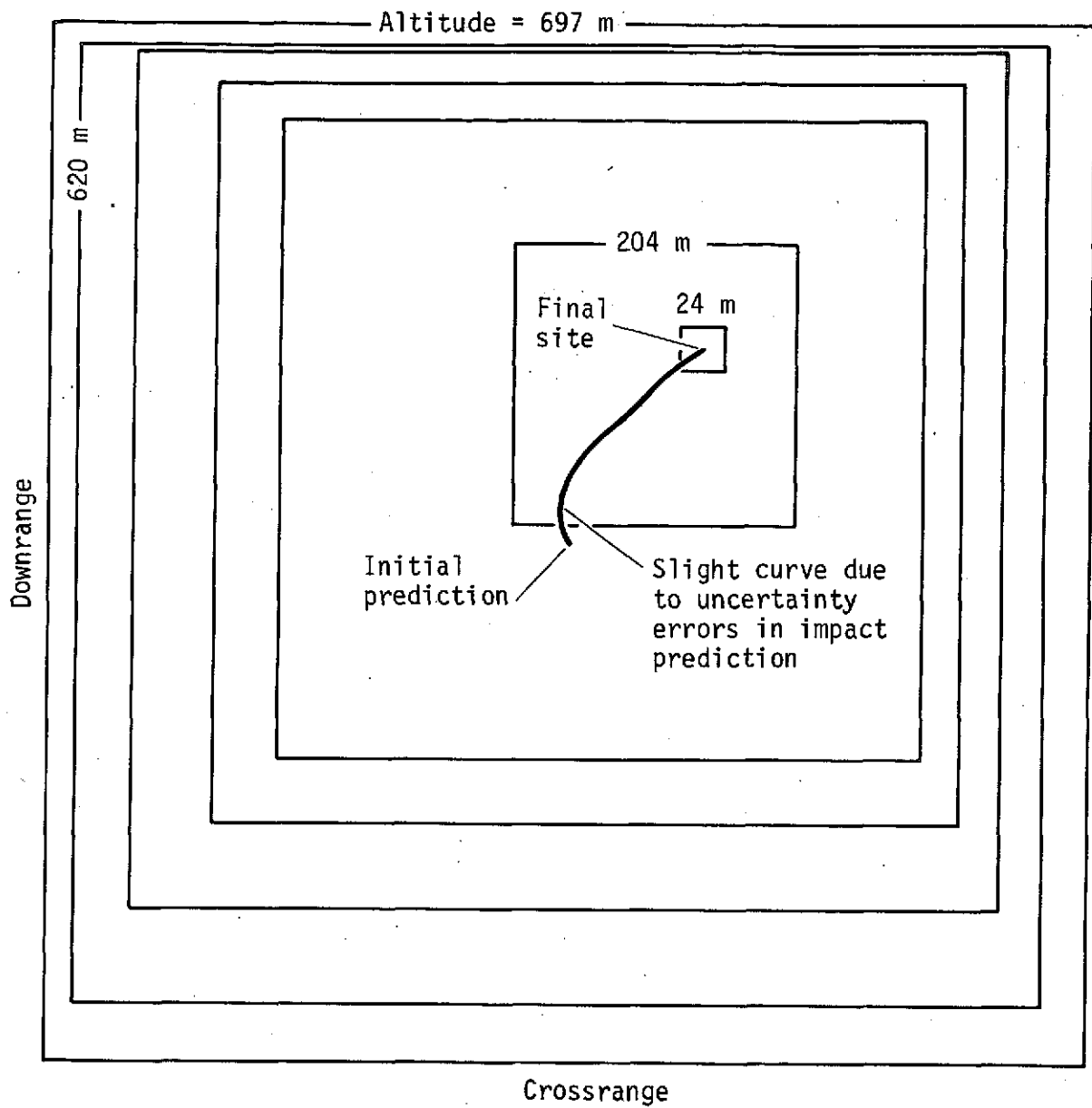


Figure 26.- Field of View Positioning Logic

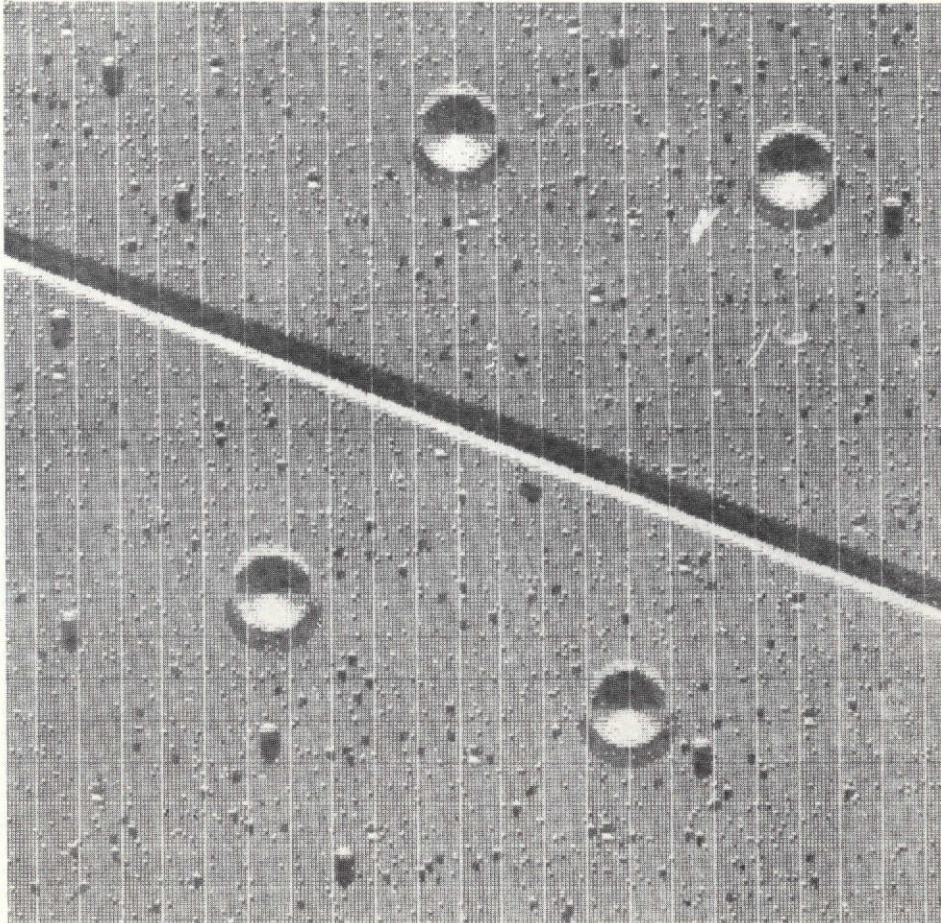


Figure 27.- Three Dimension Surface Model



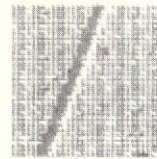
H = 697 m
Area = 213 x 213 m



621 m
207 x 207 m



550 m
189 x 189 m



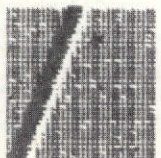
484 m
164 x 164 m



422 m
139 x 139 m



H = 364 m
Area = 116 x 116 m



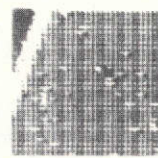
311 m
99 x 99 m



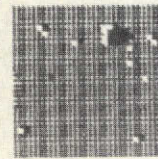
263 m
82 x 82 m



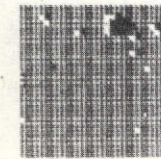
218 m
66 x 66 m



178 m
51 x 51 m



H = 142 m
Area = 39 x 39 m



111 m
29 x 29 m



83 m
21 x 21 m



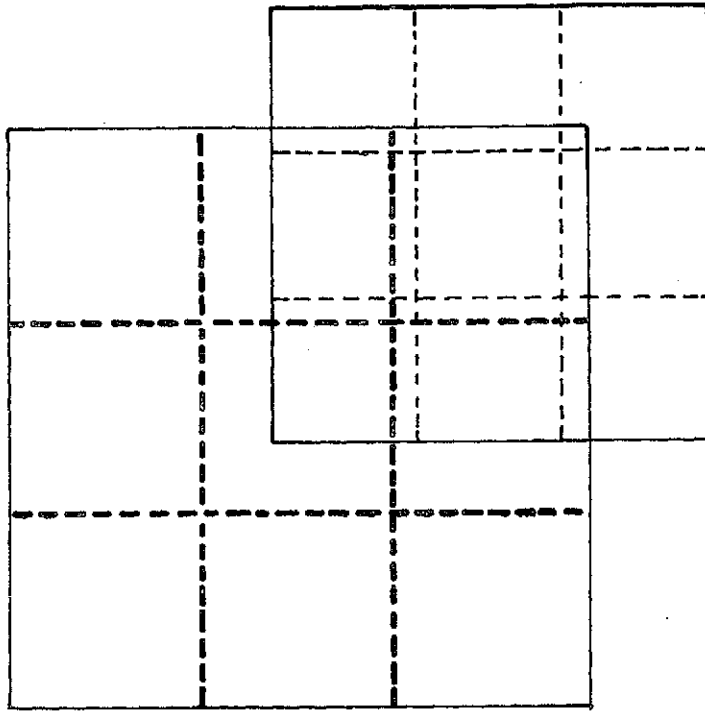
60 m
15 x 15 m



42 m
10 x 10 m

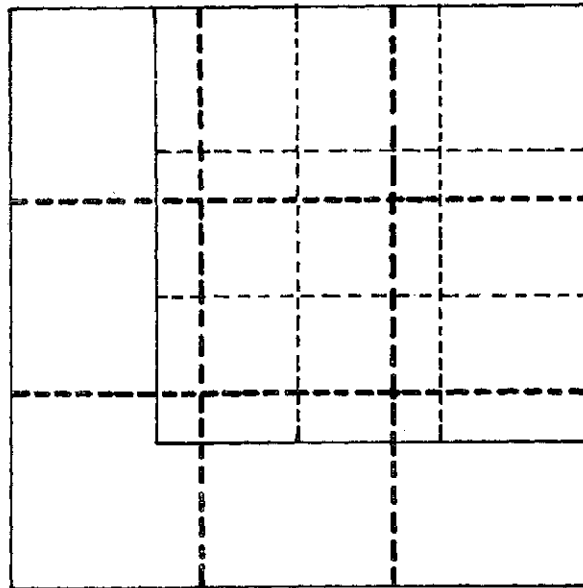


Figure 28.- MOD6MV Digital Simulation



Field of view centered
at best site

A



Field of view moved toward
best site but restricted
to original fiew of view

B

Figure 29.- Scan Positioning Logic

if it had been included in the original field of view. The scan could be restricted to the original field of view (B, Fig. 29) and moved toward the best site. This would limit maneuver range to the original field of view.

The possibilities for scan positioning are numerous. A landing site selection system should pick one that makes optimum use of video data while staying within the limits of maneuver capability.

HARDWARE AND INTERFACE REQUIREMENTS

The flight version of the optical guidance system is expected to weigh approximately 6.35 kilograms. Approximately 12 watts at 28 volts (nominal) would be required for operation. The navigation computer would be required to provide two analog or digital signals to position the middle scanned subframe at the point on the photocathode where the image of the predicted impact point is located. The computer would also be required to accept a 6-bit digital signal from the system (guidance information) and turn the system on and off. Finally, the computer would have to accept the guidance information in terms of subframe selected or desired direction of travel and effect the appropriate maneuvering.

The major functional blocks of the system are shown in figure 30.

RECOMMENDATIONS

Having successfully completed the feasibility demonstration, this section is included to suggest a cost effective approach to the further development and use of video guidance landing, and imaging system (VGLIS) technology. Due to the real time autonomous capability, simplicity of design, and potential scientific use, the VGLIS technology is particularly applicable to advanced planetary programs. It is therefore recommended that the technology be directed toward the accomplishment of the following tasks:

- 1) A mission applications study be performed to optimize the VGLIS performance for advanced planetary programs;
- 2) Further algorithm evaluation experiments be performed to extend the VGLIS capability to scientific site selection and scientific imaging;

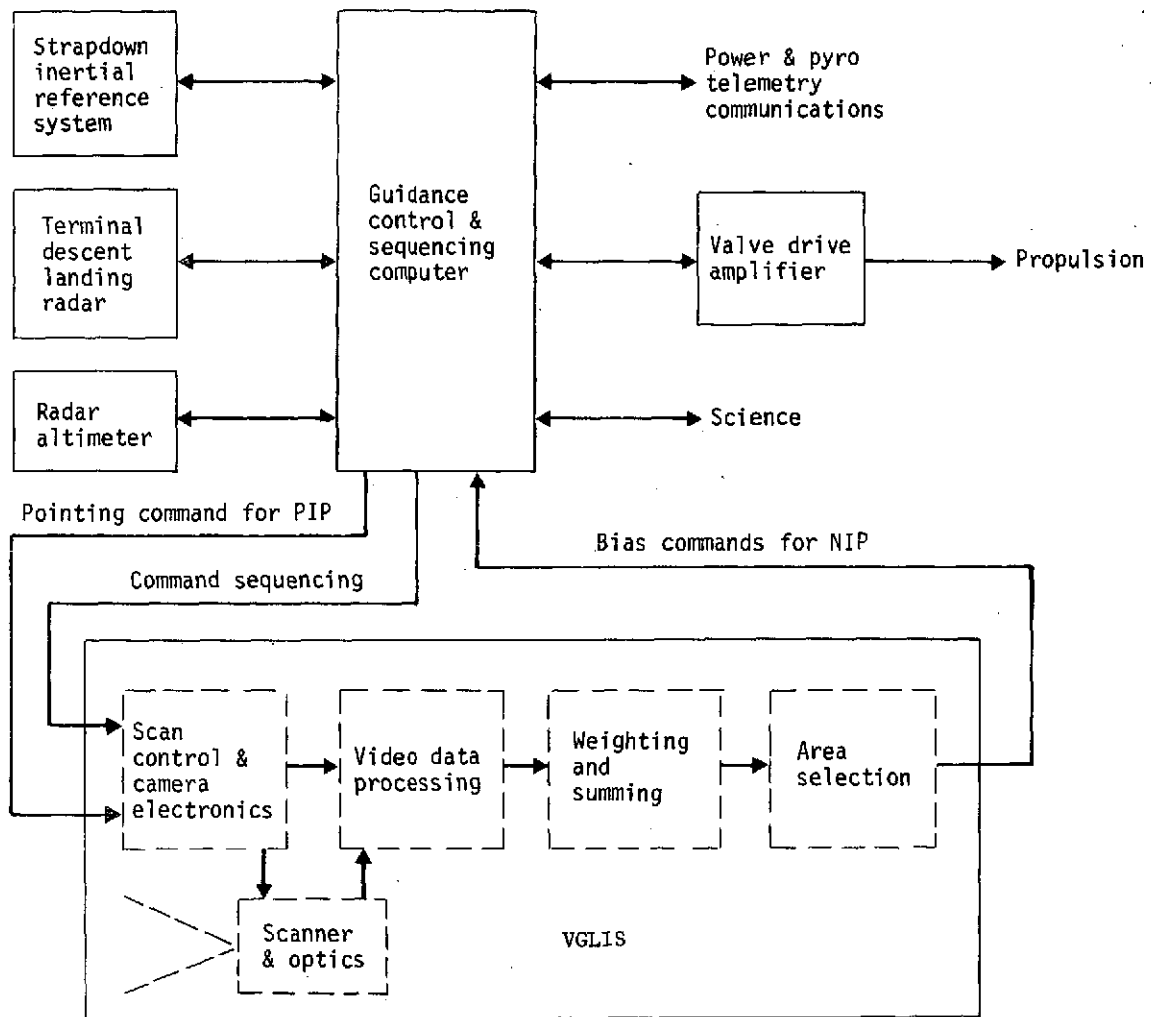


Figure 30.- Guidance and Control System Interface

- 3) The acquisition and tracking aspects of the system be investigated for terminal rendezvous guidance with solar bodies;
- 4) Terminal guidance for planetary missions be considered for footprint reduction;
- 5) The contrast sensing capabilities of the VGLIS be considered in the role of target acquisition and selection for earth resources imaging satellites.

Mission Applications Study

As a result of the VGLIS study, it is apparent that the probability of a successful landing for a planetary vehicle can be greatly increased through the addition of a video landing site selection system. Examples of potential candidates are the 1981 Mars/Viking lander, or a future Mars surface sample return mission. In considering a future Viking-type lander for any solar body, it would be necessary to address mission- and lander-peculiar requirements and constraints. Several obvious considerations are as follows:

- 1) Aeroshell effects;
- 2) Engine plume effects;
- 3) Propulsion growth capability;
- 4) Field of view requirements as a function of attitude;
- 5) Control system authority.

A substantial increase in probability of mission success for any planetary lander is a desirable goal and would more than justify the expenditure required for providing "eyes" for the lander.

Scientific Site Selection

A rationale would be established to determine the scientific relevance of proposed landing sites. Because Viking '75 and proposed follow-on Viking missions are primarily oriented toward the search for extraterrestrial life, the guide for establishing the relative merit of each site must be based on its geologic environment and the ability of that environment to support life. To this

end, the Viking '75 scientists have prepared a list of scientific criteria for site selection. These criteria are chiefly concerned with available water, high surface atmospheric pressure, porous soil, temperature anomalies, and chemical unbalance. All of these parameters require an *a priori* knowledge of the site gained from previous missions, ground-based observations, or reconnaissance surveys performed by the orbiter.

In performing this task, one would determine which terrain features, initially observed from an altitude of 1 to 2 kilometers, would indicate scientifically interesting sites. The site biasing logic would then be considered. Methods of implementing this logic into the VGLIS would be studied, along with estimating additional hardware and software requirements.

The ability to select a scientifically interesting area, maneuver to it, and then select a safe landing site implies a unique set of logic. At present the only observable is a figure of merit for roughness. For science discrimination, other observables may be required such as color, adjacent terrain characteristics (including relative elevation), relative size of safe areas, and presence or absence of periodic or other highly organized features. Color discrimination would require increasing the camera complexity. Most other observables would require an upgrading in the ability to store and process data.

Scientific Imaging

The VGLIS affords the opportunity to collect "nested" pictures of the landing site during the terminal descent phase. Nested pictures allow the scientific investigator to correlate geomorphologic features identified from orbital photographs with the features recorded by the lander camera system. This range of photo scales would permit the investigators to assess the local geologic features in the framework provided.

The system's scanning is adaptable and capable of covering all or any part of the total field of view of the instrument, currently intended to be about 60 degrees in diameter. The high data rate link from the lander to the orbiter could conceivably be made available for image information before the landing, and, in the unlikely event of a disastrous actual landing, imaging of the Mars surface before landing could prove to be invaluable to science.

The VGLIS could be switched to a full-frame scan mode during the parachute and terminal descent phase. The images would be transmitted or stored and then transmitted back to earth. The achievable benefits of imaging at lower altitudes are higher resolution, precise reconstruction of the lander impact point, and the ability to select transverses for a planetary rover. In determining the feasibility of entry imaging, it would be necessary to examine the required vehicle dynamics during the desired operating phases. Parameters such as vehicle attitude and attitude rate will affect the location of the area being scanned and possibly cause video smear due to the required finite scan time. Further investigation might reveal that the gyro outputs are required to initiate imaging during an external disturbance. The number of pictures to be taken and the selection of those to be transmitted to earth would be considered. Postflight processing would also be considered for removing the effects of smear.

In addition to considering the effects of vehicle dynamics, a graph relating ground resolution to altitude would be generated for both storage and nonstorage cameras. Potential hardware requirements for an image memory for the nonstorage-type camera should be estimated if this camera is unacceptably uplink limited.

A study to determine the minimum necessary picture bits to achieve the science objectives of these pictures should also be conducted. If only gross features are required to key the photos to high resolution orbital photos, a substantial cost savings and hardware simplification may be possible.

Terminal Rendezvous Guidance with Solar Bodies

Scientific interest in comets and asteroids stems from belief that these "small bodies" of the solar system are close to the state in which they were formed several billion years ago. Small body exploration is expected to provide decisive clues to solar system origin and evolution that cannot be found in studies of the earth, moon, and planets. These latter bodies have experienced during their evolution many catastrophic and metamorphic changes as a result of the actions of gravity, solar activity, and other dynamic processes. Consequently, all records of their early formation have been destroyed. Although considerable additional information on the nature of comets and asteroids can be obtained from more comprehensive ground-based observations, the real

breakthrough in understanding their formation and composition can only come through space flight missions to these bodies.* Initial flyby missions can be expected to provide the information necessary for planning and implementing succeeding missions for comet/asteroid rendezvous and sample return.

A common technical problem that arises in the analysis of comet/asteroid missions is related to the acquisition and tracking of a small target with generally large ephemeris errors. Although initial acquisition of a comet is enhanced by the large coma of gases and dust, the ultimate target is the nucleus that, in the case of Encke, is only about three kilometers in diameter. It has generally been concluded that successful small-body exploration--from flyby through rendezvous/dock to sample return--will require implementation of some combination of ground and onboard guidance and navigation functions, or even a totally autonomous capability to study the applicability and feasibility of an autonomous video guidance system for the accomplishment of projected comet and asteroid missions.

Landmark Navigation

Unmanned planetary landers may require a form of terminal guidance to target scientifically interesting sites and to enable footprint reduction via use of active guidance during the coast and entry phase of a given mission. This technology relates to future planetary missions such as advanced Viking, Mars sample return, and Encke, Eros, and Ceres rendezvous missions.

Target Acquisition and Tracking

Because the VGLIS has the ability to sense contrast variations, it could be used in an acquisition mode. Modifications of the current logic might enable detection of various morphological variations in a given area. As an example, earlier VGLIS experiments used edge tracking and edge repelling logic similar to that used for terminal guidance in tactical missiles.

* Fred L. Whipple, et al.: *The 1973 Report and Recommendations of the NASA Science Advisory Committee on Comets and Asteroids - A Program of Study*. NASA TM-X-71917, 1973.

Earth Resources Satellite Applications

With regard to earth-orbital missions, a coarse imaging system capable of acquiring and tracking certain surface features such as coastline, rivers, etc, is required. It would also be desirable to autonomously provide the necessary intelligence to enable the high-resolution imagery system to avoid clouds to optimize the data return and minimize processing requirements. Experiments should be performed in the laboratory in conjunction with the appropriate three-dimensional surface model to estimate the feasibility of applying the VGLIS technology to these requirements.